PHOTOPRODUCTION OF NEUTRAL PIONS IN HYDROGEN FROM 500 TO 950 MEV.

Thesis by

James Ira Vette

In Partial Fulfillment of the Requirements

For the Degree of

Doctor of Philosophy

California Institute of Technology

Pasadena, California

1958

ACKNOWLEDGEMENTS

Dr. Robert L. Walker supervised this work; his interest and many helpful suggestions have contributed materially to the success of the entire project. The assistance and guidance provided by Dr. Walker during the author's graduate residence, although fully appreciated, cannot be sufficiently acknowledged.

The constant advice and encouragement of Dr. Robert F. Bacher have been invaluable. Members of the synchrotron staff, especially Dr. A. V. Tollestrup, Dr. M. L. Sands, Dr. R. Gomez and Dr. J. M. Teem, have provided useful counsel. The author is indebted to Dr. V. Z. Peterson and Mr. Earl B. Emery for their maintenance of the liquid hydrogen target.

Many enlightening discussions with Mr. Paul L. Donoho have been the source of helpful suggestions in all phases of this work. The assistance of Mr. Walter W. Wales in all phases of this experiment is gratefully acknowledged. Mr. Howard M. Brody and Mr. Franklin P. Dixon were very useful in helping to take data. Discussions with Mr. Robert M. Worlock have proved useful. The discussions with Mr. Michel A. Bloch concerning his experimental results have been very instructive.

The synchrotron engineering staff and crew designed, constructed and maintained much of the equipment. The author is especially indebted to Mr. Dan Sell, Mr. Larry Loucks, Mr. Bruce Rule and Mr. Larry Sill in this connection.

The support of the International Business Machines Corporation through a predoctoral fellowship is appreciated. The financial support of the U. S. Atomic Energy Commission is gratefully acknowledged.

ABSTRACT

The process $\gamma + P \longrightarrow \pi^{o} + P$ has been studied by detecting recoil protons from a liquid hydrogen target which was bombarded by the bremsstrahlung beam of the California Institute of Technology electron synchrotron. The angle and momentum of the recoil protons were measured by a magnetic spectrometer-three scintillation counter coincidence system. The process has been studied between photon laboratory energies of 490 and 940 Mev. and between pion center-of-mass angles of 31.5^{o} and 147^{o}. Protons which arose from meson pair production were significant at forward laboratory angles. A correction for this contamination is discussed. The rapid decrease of the total cross section above 320 Mev. continues out to 600 Mev. and then rises slightly reaching a peak value around 800 Mev. The center-of-mass angular distributions are analyzed in a power series of the cosine of the pion angle and it is found that terms up to the fourth power are necessary to fit the data above 600 Mev. A multipole expansion is made assuming that mesons are produced in only S, P and D states; this expansion is used to show that no single multipole absorption is responsible for the rise in the cross section above 600 Mev.

TABLE OF CONTENTS

I. INTRODUCTION

The pioneering experiments of Steinberger, Panofsky and Steller (1, 2) firmly established the existence of the neutral pion and showed that the total cross section for the reaction

$$\gamma + P \longrightarrow \pi^{o} + P \qquad (1)$$

was comparable to that for charged photomeson production from hydrogen at a laboratory photon energy of 330 Mev. The measurements of Silverman and Stearns (3) and Cocconi and Silverman (4), which covered the photon energy range 200-315 Mev., indicated that the π^{o}'s are produced predominantly in a P state. The rapid rise of their excitation functions and the large magnitude of the cross section were suggestive of a resonance interaction. Since these early measurements reaction 1 has been studied extensively (5) and this early indication of a resonance behavior has been confirmed. At this laboratory the pion angular distribution for photon lab energies between 260 and 450 Mev. has been measured by Walker, Oakley and Tollestrup (6), Oakley and Walker (7), and McDonald, Peterson and Corson (8).

Walker, Oakley and Tollestrup used a photon counter and a proton counter telescope to detect one π^{o} decay gamma ray in coincidence with the recoil proton. Measurements were made with polyethylene and graphite targets and a subtraction made to obtain the cross section in hydrogen. Their method, which suffers from a low counting rate and the fact that the efficiency of the photon counter enters into the calculation of the cross section, was necessary to identify the reaction with the targets that were used.

If it can be established that the only appreciable production of protons from hydrogen comes from reaction 1, the simplest method is the detection of recoil protons from a hydrogen target. Since reaction 1 is a two body process, the measurement of the momentum and angle of the proton coupled with the knowledge of the direction of the photon beam allows one to solve the dynamical problem completely. Oakley and Walker used a magnetic spectrometer and a two counter coincidence system to measure the recoil protons from a high pressure hydrogen gas target; they were able to show that at least 98 $^{o}/_{o}$ of the protons produced in the hydrogen came from reaction 1 rather than from the competing reactions:

$$\gamma + P \longrightarrow \gamma' + P \qquad (2)$$

$$\gamma + P \longrightarrow \pi^{+} + \pi^{-} + P \qquad (3)$$

$$\gamma + P \longrightarrow \pi^{o} + \pi^{o} + P \qquad (4)$$

(Reactions 3 and 4 are only possible for photons above 320 Mev. lab energy.) Their measurements covered pion center-of-mass (C.M.) angles between 70^{o} and 150^{o}; this was extended to angles as far forward as 26^{o} by McDonald, Peterson and Corson who detected low energy protons by placing nuclear emulsions inside a hydrogen gas target. The combined data of these two experiments will be referred to as the OM data.

The results showed that the cross section exhibits a resonance type behavior with the maximum value occurring at a photon lab energy of 320 Mev. If the assumption is made that mesons are produced only

in S and P states in this energy region, the C.M. differential cross section, $\sigma(k, \theta_\pi')$, can be written

$$\sigma(k, \theta_\pi') = A_o(k) + A_1(k) \cos\theta_\pi' + A_2(k) \cos^2\theta_\pi' \qquad (5)$$

where k is the photon lab energy and θ_π' is the pion C.M. angle. An equation of this form gives a good least squares fit to the data. The results are consistent with the model first proposed by Brueckner and Case (9) that production occurs mainly by magnetic dipole absorption leading to a state of isotopic spin 3/2 and total angular momentum 3/2 together with some small S wave interference terms. The inclusion of the emulsion data showed that the electric quadrupole absorption is very small.

The purpose of the present experiment has been to investigate reaction 1 for k values between 500 and 950 Mev. The process has been studied between θ_π' values of 31.5^o and 147^o by detecting the recoil protons from a liquid hydrogen target. The momentum and angle of the proton were measured by a magnetic spectrometer and a three scintillation counter coincidence system. It was possible to keep the contribution of protons from reactions 3 and 4 small in most cases and to calculate a correction for this contamination.

In the "low" energy region a very good understanding of photo-meson production has been achieved through its relationship to the scattering problem. The dominance of the (3, 3) state has made it possible to construct successful models for low energy production.

However the region above 450 Mev. photon lab energies is devoid of theoretical predictions. The two main reasons for this are that no detailed scattering measurements other than total cross sections have been made in this region and the fact that the (3, 3) state is no longer expected to dominate. Certainly higher partial waves will become important. It is hoped that information of the π^o reaction along with the other photomeson reactions in this higher energy region can be used to suggest new models and guides to the theorists.

There are several places where the information obtained in this experiment might be useful. The data might contribute to the understanding of the peak in the I = 1/2 total cross section which has been observed by Cool, Piccioni and Clark (10) in their experiments on pion-proton total cross sections. A comparison with the results of Bloch and Sands (11), who have studied the photoproduction of π^-'s from hydrogen, can give an indication of the ratio of single to multiple meson production at these energies. Both of these points will be discussed further in Section X. The knowledge of the photomeson cross sections at high energy can also be used to more correctly evaluate dispersion integrals such as those that appear in the calculation of Compton scattering. (12).

II. EXPERIMENTAL APPARATUS

The experimental area of the California Institute of Technology electron synchrotron laboratory is shown in figure 1. The circulating electron beam strikes a .031 inch thick tantalum radiator once each second, this being the repetition period of the synchrotron. The beam is "dumped" slowly by tailoring the R.F. amplitude so that each beam pulse lasts about 20 milliseconds. During this time the magnetic field of the synchrotron is maintained at constant value to give a fixed bremsstrahlung end point energy. The resultant photon beam passes out of the machine through a primary lead collimator; it then goes through the high pressure gas target, a secondary collimator, the liquid hydrogen target, and finally into the beam monitor. An 8 inch lead scraper wall is used down beam from the primary collimator to block, without further collimation, any beam splatter from the primary collimator. A similar 4 inch wall is used down beam from the secondary collimator for the same purpose. A series of radar magnets placed after the secondary collimator is used to sweep out charged particles generated by the beam in passing through the gas target and the secondary collimator. A large amount of concrete shielding is used around the machine to reduce the general background.

The primary collimator used during this experiment was made of a 12 inch long, tapered, lead cylinder with a tapered hole of 1.9 cm. maximum diameter. The secondary collimator, which was made in a similar manner, contained a tapered rectangular hole of maximum dimensions 5.1 cm. x 4.1 cm. The resultant beam size at the liquid

Figure 1. Plan View of Experimental Area.

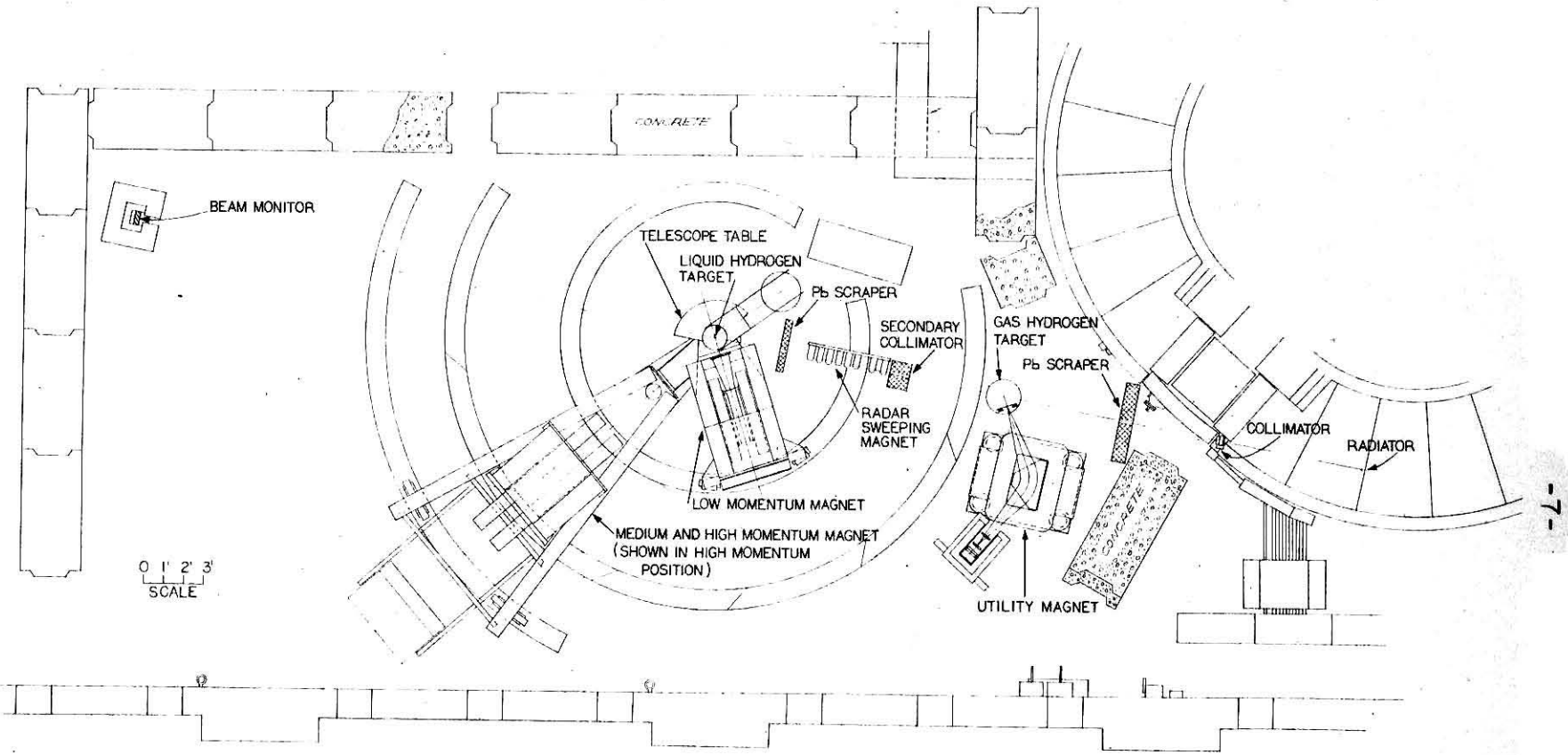
CONCRETE
BEAM MONITOR
TELESCOPE TABLE
LIQUID HYDROGEN TARGET
Pb SCRAPER
SECONDARY COLLIMATOR
GAS HYDROGEN TARGET
Pb SCRAPER
RADAR SWEEPING MAGNET
COLLIMATOR
RADIATOR
LOW MOMENTUM MAGNET
MEDIUM AND HIGH MOMENTUM MAGNET (SHOWN IN HIGH MOMENTUM POSITION)
UTILITY MAGNET
CONCRETE
0 1' 2' 3'
SCALE

hydrogen target was 6.6 cm. vertical height and 5.5 cm. horizontal width. The spatial density of the beam at this point was obtained by measuring the density of blackening of 400 micron Ilford G-5 nuclear emulsions which had been exposed to the beam behind a 1/8 inch lead plate.

In order to study the π^o reaction, recoil protons from the liquid hydrogen target were measured in this experiment. The target, which was designed by Dr. V. Z. Peterson, is shown in figure 2. It consists of a 3 inch diameter, 5-1/2 inch long, cylindrical cup made of .003 inch Mylar. This cup is surrounded by a series of cylindrical copper and aluminum radiation shields, the smallest having a diameter of about 8-1/2 inches. The region between the cup and a .024 inch Mylar, 360^o, external window is maintained under a high vacuum. A 10 liter liquid hydrogen reservoir, which is surrounded by a 26 liter liquid nitrogen reservoir (both partially shown in figure 2), sits concentrically above the cup. Hydrogen gas which flows through the center of this reservoir is condensed in the cup and remains in this state by heat exchange with the liquid hydrogen reservoir. Particles originating in the target must penetrate .027 inch of Mylar, .003 inch of copper and .0005 inch of aluminum before reaching the outside.

The detection system is shown in figure 3. Charged particles which emerged from the target within a specified solid angle were momentum analyzed by a uniform field, wedge shaped magnetic spectrometer and focussed on a three scintillation counter array. Protons were identified by their energy loss in these counters. The

Figure 2. Liquid Hydrogen Target.

This figure shows the bottom portion of the target which is suspended below the liquid hydrogen and liquid nitrogen reservoirs. The center line of the target is directly over the pivot point of the magnets. For more details of the target see Drawing 13 M 792A.

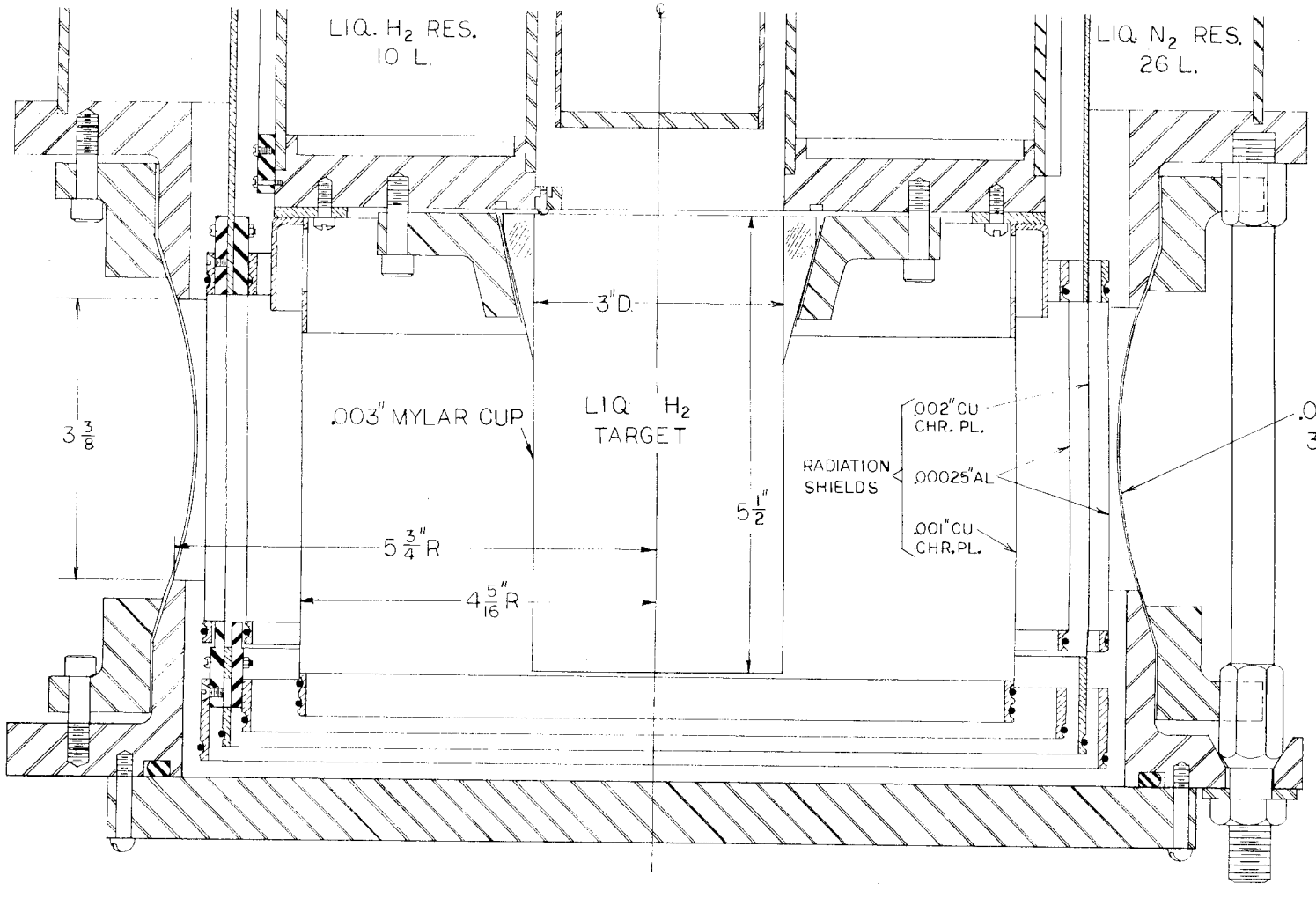
LIQ. H_2 RES.
10 L.
LIQ. N_2 RES.
26 L.
3" D
.003" MYLAR CUP
LIQ H_2
TARGET
$3\frac{3}{8}$
$5\frac{1}{2}$"
$5\frac{3}{4}$" R
$4\frac{5}{16}$" R
RADIATION
SHIELDS
.002" CU
CHR. PL.
.00025" AL
.001" CU
CHR. PL.
.024" MYLAR
360° WINDOW

Figure 3. Experimental Layout.

This figure shows a cross sectional view taken through the median plane of the magnet. This particular arrangement shows the medium momentum magnet. The arrangements with the low and high momentum magnets are very similar, the main difference being the magnet-target and counter-magnet distances. The lead slit was not used with the low momentum magnet.

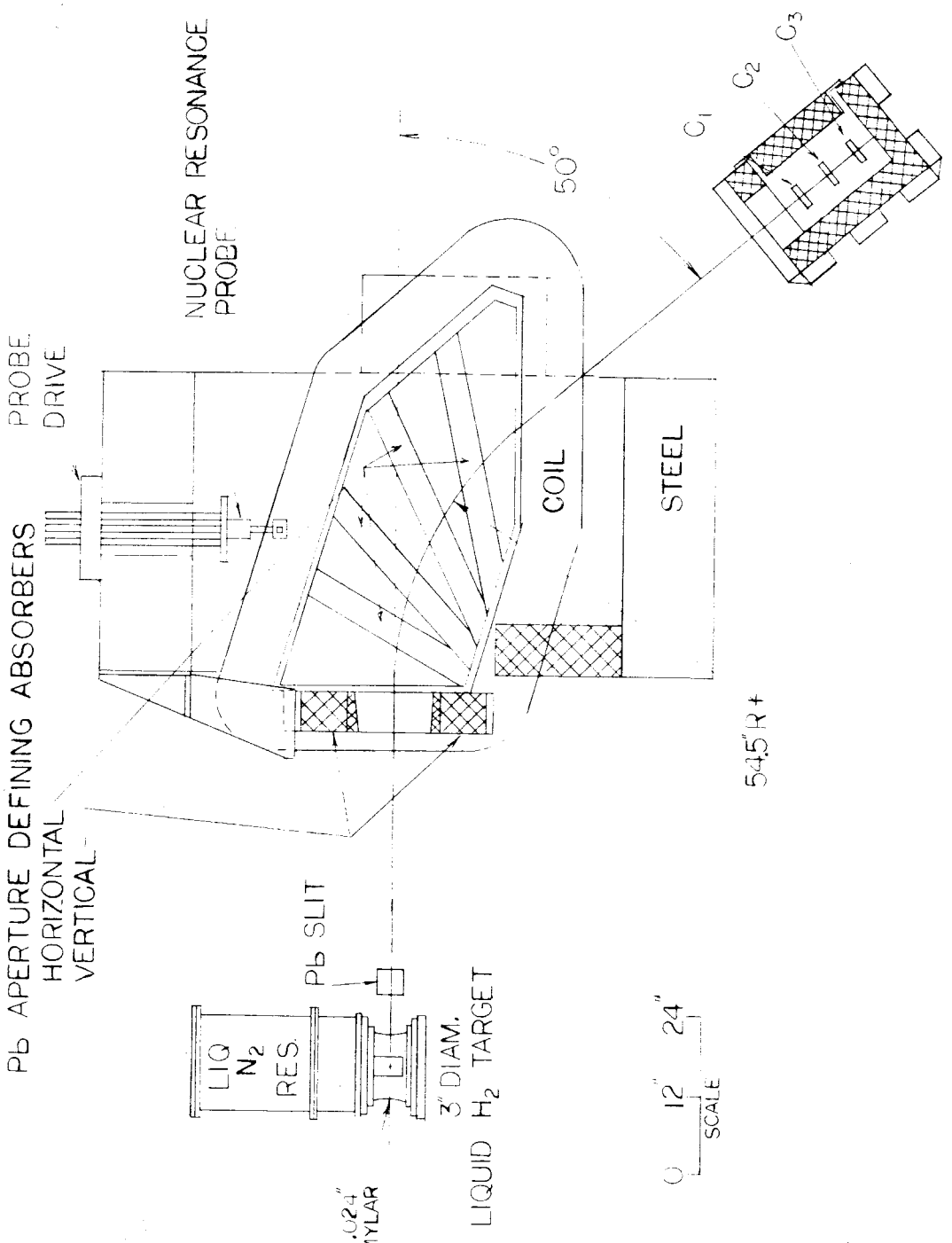
Pb APERTURE DEFINING ABSORBERS
HORIZONTAL
VERTICAL
PROBE DRIVE
NUCLEAR RESONANCE PROBE
50°
C_1
C_2
C_3
COIL
STEEL
5.45" R +
Pb SLIT
LIQ N_2 RES.
3" DIAM. LIQUID H_2 TARGET
.024" MYLAR
0 12" 24"
SCALE

spectrometer solid angle is defined in the vertical direction by a 6 inch thick lead slit mounted on the front aperture of the magnet. The faces of the slit are tapered to point toward the center of the target in order to minimize scattering and slit penetration. The solid angle is defined in the horizontal direction by a system of lead slits which are attached to the magnet pole tips. The position and size of these slits are such that particles scattering off the pole tip faces will either miss the counters or be blocked from them by one of the slits. The magnetic field, which is produced by a current regulated D.C. generator, was measured and monitored by a proton resonance magnetometer during the whole experiment. With this apparatus it is possible to measure and maintain the magnetic field to an accuracy of 0.1 $^{o}/_{o}$.

Three different magnetic spectrometers were used in the course of the experiment. These are referred to as the low, medium and high momentum magnets. The high momentum magnet is made by attaching a pole tip modification to the medium momentum magnet and repositioning it with respect to the target. The same set of counters was used with these two magnets. The low momentum magnet is equipped with a stainless steel vacuum chamber that encloses the counters and extends to within 8 inches of the external window of the target in order to measure low energy protons. The medium-high momentum magnet was designed by P. L. Donoho; the low momentum one was designed by J. I. Vette. The characteristics of these spectrometers have been measured very carefully by means of the stretched wire technique. Since these measurements are discussed in detail elsewhere (13, 14),

only some of the results will be listed in Table I for reference.

TABLE I.

Magnet	P_{max}(Mev/c)	Solid Angle	$\Delta P/P$	Width of $\Delta P/P$ Defining Counter
Low	275	.0194	.081	3.8 in.
Medium	600	.0075	.098	4.75 in.
High	1200	.00243	.099	4.75 in.

To improve the angular resolution for a given solid angle, the magnets deflect the particles in a vertical plane. Each magnet is mounted on a frame which is supported at one end by a set of wheels which roll on steel tracks. The other end of the frame is supported by a roller bearing pivot which is centered on the axis of the liquid hydrogen target. The counters for the medium-high momentum magnet are mounted in a 4 inch lead house which is attached to the magnet frame. The low momentum magnet counters are mounted in the vacuum chamber and 4 inches of lead is stacked around this section of the chamber. This arrangement makes it very easy for one person to manually change the angular position of either magnet without removing any shielding. Angular marks along the tracks have been surveyed in every 10^{o}. An angle measuring device attached to the magnet frame interpolates between these marks. With this arrangement the angular position of the magnet can be set to within $\pm$ 0.05^{o}.

All the scintillation counters were made with a polystyrene base plastic scintillator material obtained from the University of California Radiation Laboratory at Livermore. Each counter was viewed on two ends through lucite light pipes by RCA type 6655 photomultipliers. One-half mil bright aluminum wrapped around the scintillator served as a reflector. The outputs of the two phototubes which viewed a single counter were balanced and then connected in parallel. The medium-high momentum magnet counters were 11 inches long; two of these were 2 cm. thick and the other was 1 cm. in thickness. P. L. Donoho has measured the resolution of these counters with 486 Mev/c pions and protons. The results of this measurement were:

$$\sigma_\pi\,(2\text{ cm.}) = 0.15\ \mu_\pi\,(2\text{ cm.}) \qquad \sigma_p\,(2\text{ cm.}) = 0.06\ \mu_p\,(2\text{ cm.})$$

$$\sigma_\pi\,(1\text{ cm.}) = 0.21\ \mu_\pi\,(1\text{ cm.}) \qquad \sigma_p\,(1\text{ cm.}) = 0.08\ \mu_p\,(1\text{ cm.})$$

where σ is the standard deviation and μ is the mean pulse height. The low momentum magnet counters were 8-1/2 inches long; the front counter (C-1 in figure 3) was .16 cm. thick and the central one was 1.1 cm. The highest momentum protons that were measured with this spectrometer stopped in the central counter. Since the protons lost at least 5 times as much energy as the mesons for the low momentum runs, there was no problem in distinguishing the two types of particles. The standard deviation of the proton pulses in the 0.16 cm. counter was about 30 ^{o}/o of the mean pulse height for protons in the momentum range 200-275 Mev/c.

The electronic circuits utilized in this experiment are shown in figure 4 along with the Synchrotron Lab drawing number of each one. The two paralled outputs of the photomultipliers which viewed a single counter were fed into an integrating preamplifier where the pulses were shaped by a shorted delay line into 0.5 microsecond rectangular pulses. The preamplifier outputs were amplified by 0.07 microsecond rise time pulse amplifiers and fed into both a delay line mixer and a 6 channel gated discriminator. (It is necessary to gate the counting equipment so that it is on only for the short period when the electron beam is striking the radiator; this eliminates the many transients which occur during injection time and reduces cosmic ray background.) The delay line mixer delayed inputs 1, 2 and 3 by 0.5, 1.5 and 2.5 microseconds, respectively. The single output of this circuit was fed into the vertical amplifier of an oscilloscope. The outputs of the 6 channel discriminator were fed into a 6 channel coincidence-anti-coincidence circuit which had a resolving time of 0.15 microsecond. The pulses from C-1, C-2 and C-3 were placed in coincidence (referred to as 1.2.3) except for those runs where the protons could only penetrate the first two counters; in this case a 1.2 coincidence was used. In normal operation a 1.2.3 (or 1.2) pulse triggered the horizontal sweep of the oscilloscope and the resulting trace, which displayed the pulse heights of all three counters, was photographed. Time exposures containing of the order of 50 traces each were made and used to help set the biases properly to discriminate against pions but not protons. The accidental rate was obtained by delaying the

Figure 4. Block Diagram of the Electronic Apparatus.

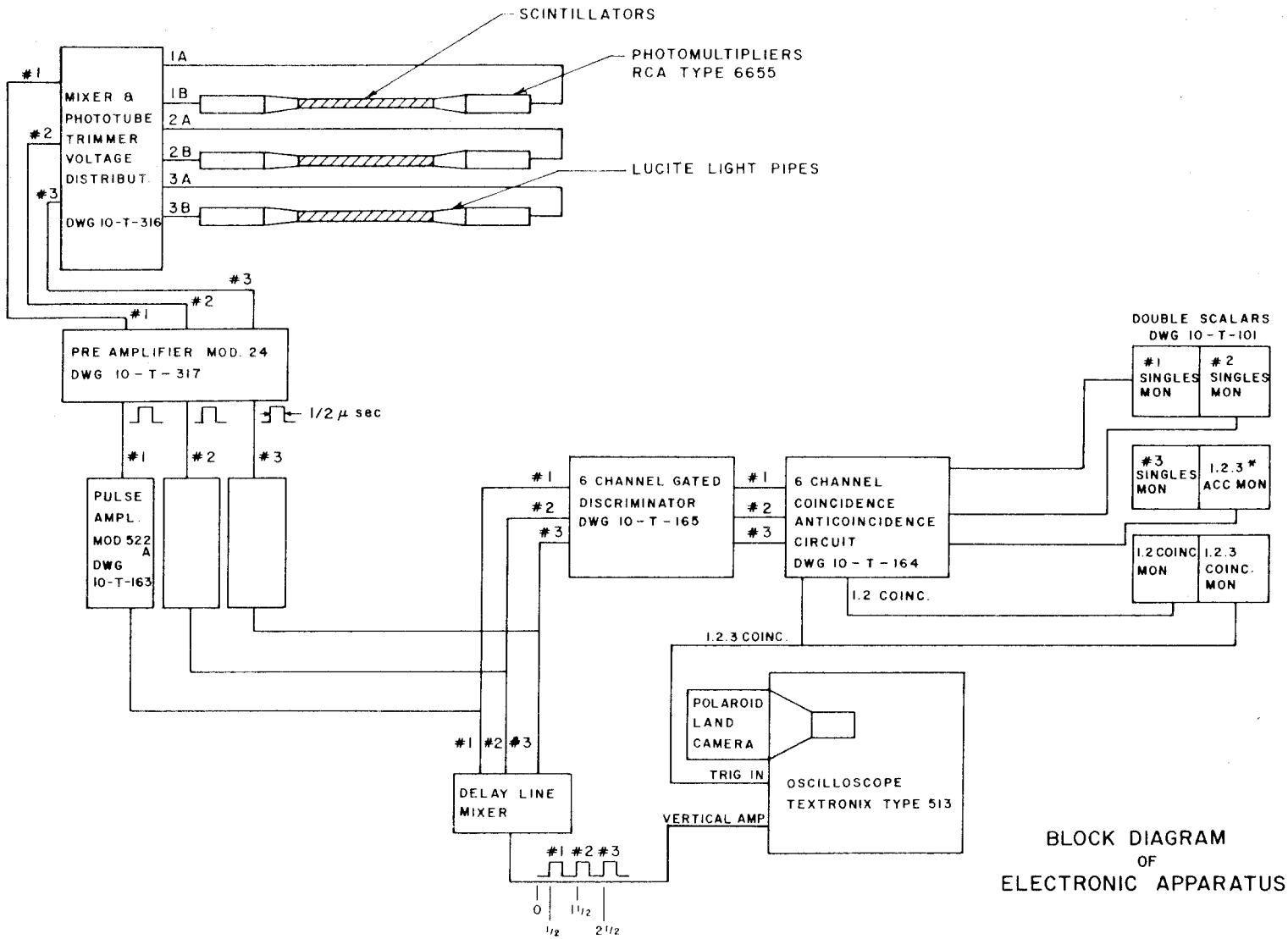

BLOCK DIAGRAM
OF
ELECTRONIC APPARATUS

output of the rear counter one microsecond and putting it in coincidence with a 1.2 coincidence (referred to as 1.2.3*). The 1.2.3* rate (or 1.2*) was negligible for all the runs. Protons were selected by raising the discriminator biases to exclude mesons. Scalers were used to record the desired counting rates.

The synchrotron beam monitor is a thick walled Cornell type, air ionization chamber. The response of this chamber as a function of the peak energy of the bremsstrahlung has been measured and will be discussed later.

III. EXPERIMENTAL PROCEDURE

Since the reaction under investigation is a two body process, the photon lab energy, k, and the meson C.M. angle, θ'_π, can be calculated once the lab momentum, P, and the lab angle, θ_p, of the recoil proton are known. To make a run the magnet angle and central momentum were set to correspond to a desired k, θ'_π value. Then the biases on the discriminators were raised until only proton pulses were seen on the photographed oscilloscope traces. Pictures were taken during all the runs to make sure that no mesons were counted and no protons were missed. In general, a series of points corresponding to a constant k and various values of θ'_π were run with hydrogen in the target; then the points were repeated with no hydrogen in the cup to obtain the background counting rate. When another value of k was investigated, the same values of θ'_π were chosen. In this manner the angular distribution functions and the excitation functions for a constant θ'_π were measured directly.

When a gamma ray in the energy range 500-1100 Mev. strikes a hydrogen target, protons can arise from the reactions:

$$\gamma + P \longrightarrow \gamma' + P \qquad (1)$$

$$\gamma + P \longrightarrow \pi^o + P \qquad (2)$$

$$\gamma + P \longrightarrow \pi^+ + \pi^- + P \qquad (3a)$$

$$\gamma + P \longrightarrow \pi^o + \pi^o + P \qquad (3b)$$

$$\gamma + P \longrightarrow 3\pi\text{'s} + P \qquad (4)$$

$$\gamma + P \longrightarrow 4\text{-}5\pi\text{'s} + P \qquad (5)$$

Of course there are also protons produced in the Mylar cup which holds the hydrogen; this background from the target will be discussed later.

It is possible to eliminate the contamination from reactions 4 and 5 and to reduce that which comes from reaction 3 at most points by running with the maximum energy of the bremsstrahlung, E_o, about 100 Mev. above the k value being investigated for reaction 2. This will be illustrated by the situation depicted in figure 5. Here it is desired to study reaction 2 at k = 800 Mev. The rectangle represents the window in P, θ_p space that the magnetic spectrometer-scintillation counter system provides. The value for E_o is chosen to be 940 Mev. The curves drawn for reactions 3 and 4 are computed on the assumption that the mesons go off together; consequently these lines represent the maximum momentum that protons from reactions 3 and 4 can have at the given lab angle, θ_p, with the machine running at E_o = 940 Mev. If the bremsstrahlung cutoff at E_o were very sharp, the optimum situation would be to lower E_o until the curve $k = E_o$ for reaction 2 just begins to intersect the top of the P, θ_p window. A further reduction of E_o would result in a undesirable loss in counting rate.

Because the energy spectrum of the bremsstrahlung beam had not been measured at the time these data were taken, the optimum setting of E_o was never realized. In order to make this point clear,

Figure 5. Kinematics for the Photoproduction of One, Two and Three Mesons in Hydrogen.

The solid curves give the proton laboratory momentum versus laboratory angle for the $\gamma + P \longrightarrow \pi^o + P$ reaction at the constant photon energies of 800 and 940 Mev. The curves for the other two reactions are calculated on the assumption that the 2 or 3 mesons are emitted together. These curves give the maximum momentum that protons from the reactions $\gamma + P \longrightarrow 2\pi$'s $+ P$ and $\gamma + P \longrightarrow 3\pi$'s $+ P$ can have at a given laboratory angle if the machine energy is 940 Mev. The shaded region represents the sensitive region provided by the detection system when the magnet is set at the angle and momentum shown. For a discussion of this figure see page 21.

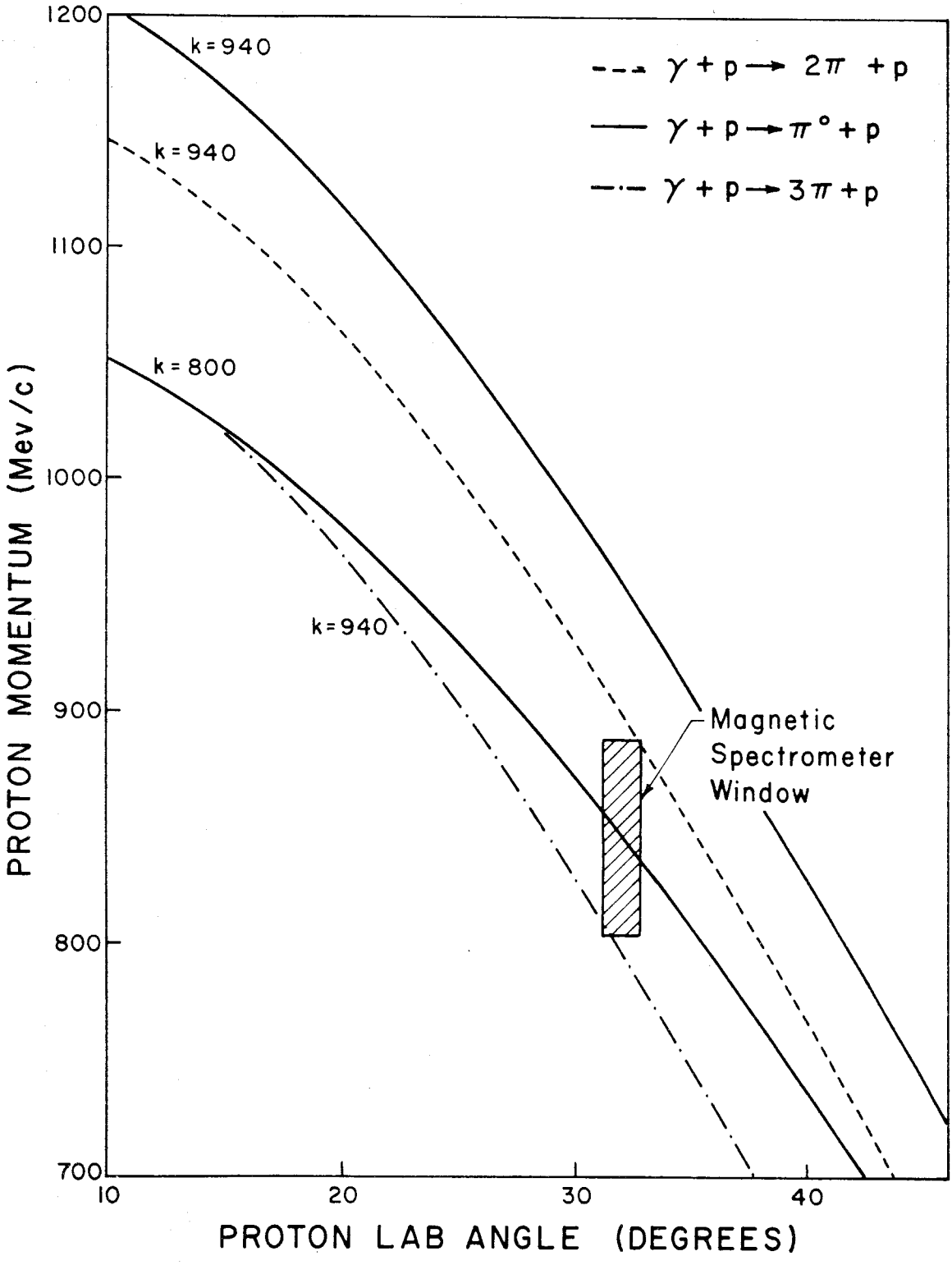
1200
1100
1000
900
800
700
10
20
30
40
PROTON MOMENTUM (Mev/c)
PROTON LAB ANGLE (DEGREES)
k=940
k=940
k=800
k=940
γ + p → 2π + p
γ + p → π° + p
γ + p → 3π + p
Magnetic
Spectrometer
Window

a discussion of the energy spectrum and its measurement will now be made.

The number of photons within the energy interval k to k + dk, N(k)dk, is given by

$$N(k)dk = \frac{Q}{k} B (k/E_o, E_o)dk \qquad (6)$$

where Q is a quantity that is independent of k and will be discussed later. The function $B(k/E_o, E_o)$, which is used to describe the spectrum, is normalized so that

$$\int_o^1 B(t, E_o)dt = 1 \qquad (7)$$

where $t = k/E_o$. The tantalum radiator of the synchrotron is 0.2 radiation length thick and so constitutes a "thick" target. D. D. Elliott (15) has made a calculation of the spectrum to be expected from this target; his $B(t, E_o = 1000$ Mev.) is shown in figure 6. Recently the spectrum has been measured by Dr. R. L. Walker, P. L. Donoho and E. Emery (16) with a pair spectrometer. Although the results have not been fully analyzed yet, the preliminary calculations indicate a spectrum similar to that of a "thin" target. At the high energy end, $k \approx E_o$, the measured spectrum falls off rapidly; the step is almost as steep as possible for the known energy resolution of the spectrometer. Until this upper end is better analyzed, it is approximated by a sharp step in figure 6 which gives the preliminary measured $B(t, E_o = 1000)$ used in analyzing the π^o data. The fact that the cutoff is shown as a

Figure 6. Bremsstrahlung Spectrum Function $B(k/E_o, E_o = 1000$ Mev.)

The dotted curve is the function calculated by Elliott (15) for the 0.2 radiation length tantalum target used in the synchrotron. The solid curve, which was abstracted from the pair spectrometer measurements of Walker, Donoho and Emery (16), was used in the data reduction of this experiment. For a further discussion see page 24.

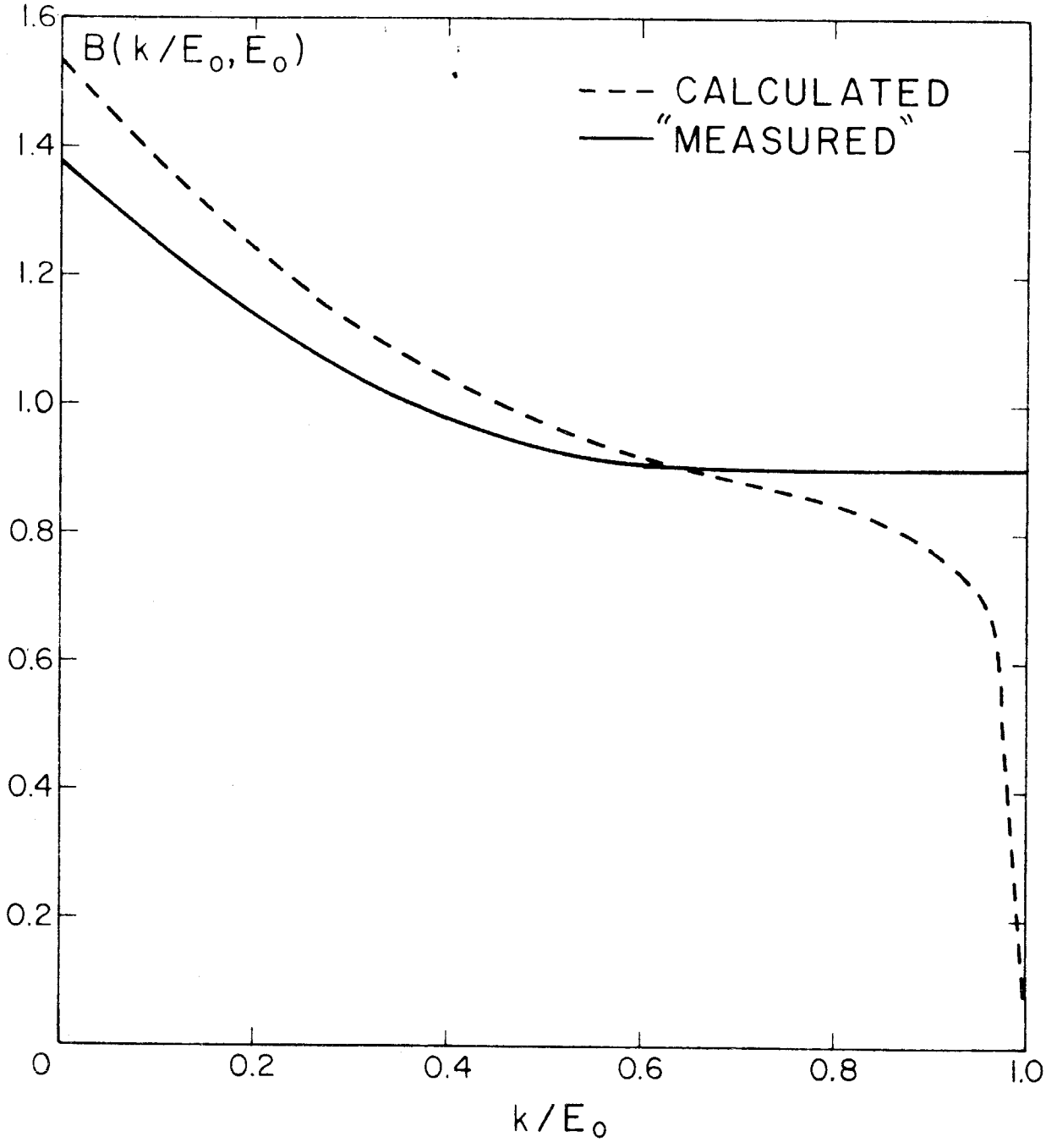
B(k/E₀, E₀)
--- CALCULATED
—— "MEASURED"
1.6
1.4
1.2
1.0
0.8
0.6
0.4
0.2
0
0.2
0.4
0.6
0.8
1.0
k/E₀

discontinuous step will have no effect on any experiment which has a poorer photon energy resolution than the 2 °/o resolution of the pair spectrometer system. Since the spectrum was previously believed to be roughly that calculated by Elliott, it was decided to make the runs with a slightly higher value of E_o than the optimum case for a sharp cutoff. In order to be compatible with other experiments that were being done at the same time, E_o was generally a compromise value determined by the various experiments.

The five k values investigated by this experiment were centered around 500, 600, 700, 800 and 950 Mev. and the corresponding E_o values were 720, 720, 820, 920-940 and 1080 Mev. for most of the runs. A correction for the contamination of reaction 3 has been calculated and will be discussed later. The smallness of the contribution of protons from reaction 1 will also be discussed at that time.

For momenta above 850 Mev./c the ratio of the energy lost by protons to that lost by mesons in the counters becomes less than 1.5 and the two peaks can no longer be clearly resolved. Below this value a proper setting of all three discriminator biases allows one to reject mesons without cutting into the proton peak. (One set of runs with a thick lucite target in the beam revealed a deuteron peak clearly separated from the proton peak.) Fortunately a more elaborate pulse height analysis was not necessary in this experiment to measure protons above 850 Mev./c. The highest momentum mesons produced in hydrogen at a given lab angle are made by the peak energy photons in the reaction

$$\gamma + P \longrightarrow \pi^+ + N \qquad (8)$$

The kinematics of this reaction are plotted in figure 7 for photon energies corresponding to the E_o values that were used in this experiment. The kinematics for reaction 2 are plotted for the photon energies which were investigated. The size of the spectrometer-scintillation counter window was such that no mesons produced in hydrogen could get into the counters through the magnet in this experiment when protons above 850 Mev./c were measured.

The temperature of the beam monitor, atmospheric pressure and E_o, which was obtained by measuring the magnetic field of the synchrotron during beam dump, were recorded periodically. Different runs for the same point taken a week apart checked very well in most cases. Sufficient background runs were taken at each point to minimize the relative counting error for a given integrated beam intensity. A lead slit, 3-3/4 inches wide placed 11 inches from the center of the target (see figure 3), was used for all the runs taken with the medium momentum magnet and most of those taken with the high momentum magnet. The slit was used to reduce the background which came from the region of the external window of the target that was bombarded by the photon beam. Runs with and without the slit were made to check that no additional protons from the hydrogen were scattered into the magnet by this slit.

Figure 7. Kinematics for Photoproduction of a Single Meson in Hydrogen.

The dotted curves give the π^+ laboratory momentum versus laboratory angle at constant photon energies for the $\gamma + P \longrightarrow \pi^+ + N$ reaction. The solid curves give the proton laboratory momentum versus laboratory angle for the $\gamma + P \longrightarrow \pi^o + P$ reaction. The peculiar selection of k values is explained on page 27.

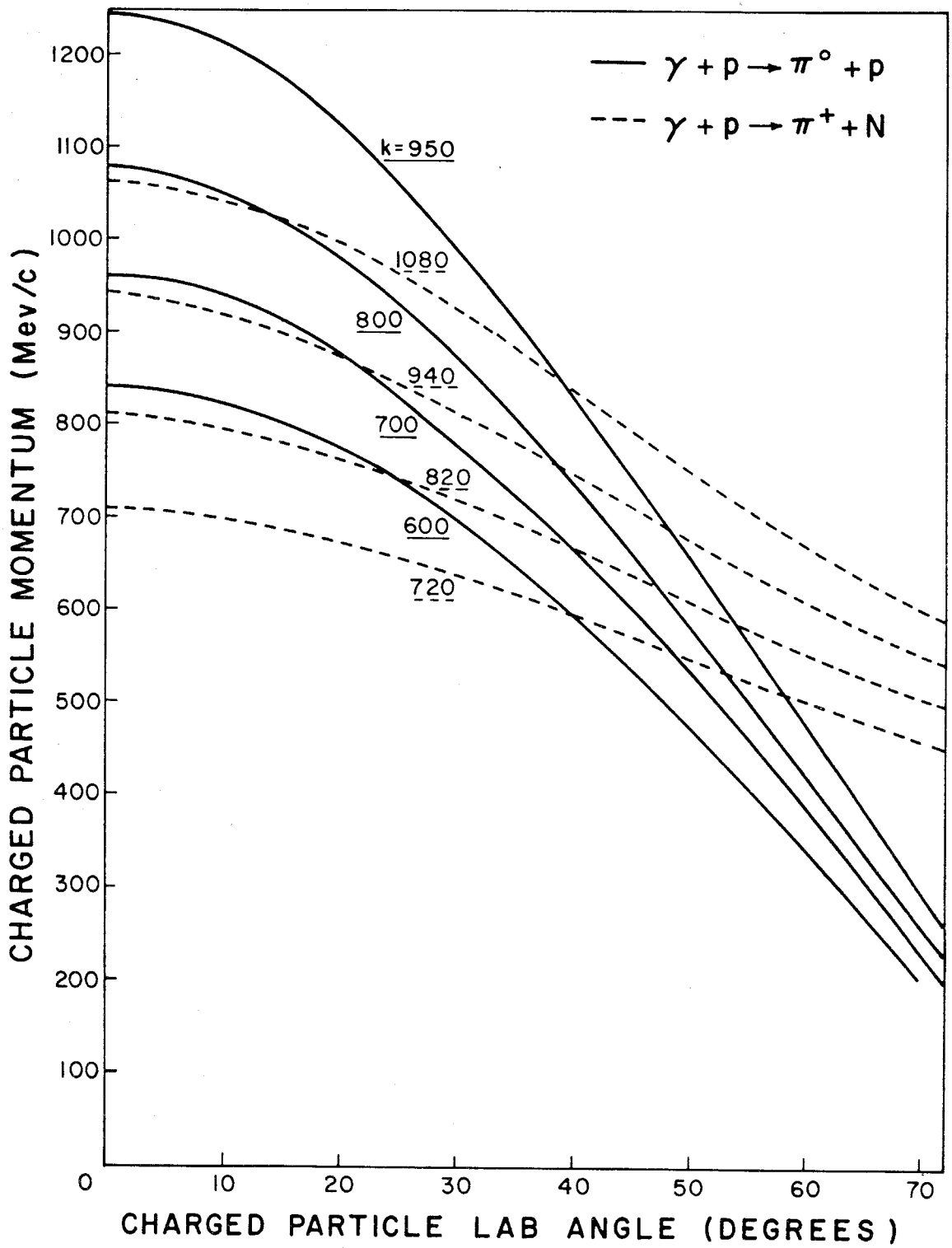
$\gamma + p \rightarrow \pi^\circ + p$
$\gamma + p \rightarrow \pi^+ + N$
k=950
1080
800
940
700
820
600
720
CHARGED PARTICLE MOMENTUM (Mev/c)
CHARGED PARTICLE LAB ANGLE (DEGREES)
0
100
200
300
400
500
600
700
800
900
1000
1100
1200
10
20
30
40
50
60
70

IV. BACKGROUNDS

The main background counting rate came from photoprotons produced in the 3 mil Mylar cup. Measurements were made with a carbon target and a hollow Mylar cylinder the same size as the cup to check that the magnitude and the energy dependence of the background were consistent with protons produced in Mylar. Most of the background from the radiation shields and the external window was eliminated by the slits described in the previous section. Unfortunately this latter source was not realized during the low momentum magnet runs, which were made at the beginning of the experiment. The fact that these runs were made without a slit and that the cross section for the photoproduction of low energy protons in Mylar is large resulted in an empty target rate that amounted to 50 - 60 $^{o}/o$ of the full target rate. The background rate for the medium momentum magnet runs was 10 - 30 $^{o}/o$ of the hydrogen runs.

There were two additional sources of background for many of the points taken with the high momentum magnet. Cosmic rays represented about 20 $^{o}/o$ of the counts. This was taken into account by recording the time of each run and the length of the pulse used to gate the discriminator circuit. The cosmic ray rate was measured under the same conditions as the full target runs. Several of the runs taken at $\theta_p = 15^{o}$ and 20^{o} had background counts which arose from the production of electrons in the hydrogen which were scattered by the air into the counters. Since the protons coming through the magnet were nearly minimum ionizing, it was not possible to distinguish the

electrons from the protons by pulse height analysis. Although the lead shielding around the counters eliminated most of this source of background, more shielding could have reduced it even further. This fact was not discovered until after the full target runs had been made. This additional background was measured by blocking up the magnet aperture with 10 inches of lead and making both full and empty target runs under the same conditions as the regular runs. The counting rate difference between these two types of runs was added to the normal empty target rate to obtain the complete background. This additional rate amounted to 20 $^{o}/o$ of the total background rate. The total background rate was 10 - 30 $^{o}/o$ of the full target runs.

V. DATA REDUCTION

The output of the 1 inch copper air ionization chamber is fed into an ion current integrator; the unit of integrated beam intensity is called a BIP, the abbreviation for beam integrator pulse. The total amount of beam energy in Mev., U, which must pass through the ion chamber to give one BIP depends on the ion chamber temperature, the atmospheric pressure, the maximum energy of the bremsstrahlung, and the constant of the integrator circuit. Using the ideal gas law to correct for temperature and pressure, one can write

$$U(E_o, T, P) = K_o(E_o) \frac{T p_o M}{T_o p} \qquad (1)$$

where $K_o(E_o)$ is the response of the ion chamber in Mev./coulomb at standard temperature and pressure, M is the integrator calibration in coulomb/BIP, T is the temperature in degrees Kelvin and p is the pressure in mm. of Hg. It is convenient to denote

$$U(E_o, T_o, p_o) \equiv U_o \equiv K_o(E_o) M_s \qquad (2)$$

where M_s is the calibration for the standard integrator.

Dr. R. Gomez (17) has measured $K_o(E_o)$ using the energy independent multiple plate chamber designed by Wilson (18) and has calibrated the ion current integrator. The values of K_o obtained were 4.45, 5.05, 5.41 x 10^{18} Mev./coulomb at E_o = 497, 789, 1080 Mev., respectively. The value for M_s was 2.22 x 10^{-7} $\pm$ 0.5 % coulomb/BIP.

In many cases several runs taken at the same k, θ_π'-point had slightly different values of T, p and E_o indicated by primes. Instead of using the number of BIPs, N, for a run taken with an integrator whose calibration constant was M, the quantity

$$N^* = \frac{N\, T'\, p_o\, M\, U_o(E_o')\, E_o}{T_o\, p'\, M_s\, U_o(E_o)\, E_o'} \tag{3}$$

was used to divide into the total number of counts that remained after cosmic rays were subtracted to obtain the counting rate, C'. The counting rate obtained by subtracting the background and contamination rates from C' will be denoted by C.

It is possible to convert C into an average C.M. differential cross section. Consider an element of volume dxdydz in the hydrogen target where x and y are coordinates transverse to the direction defined by the photon beam and z is along the beam. The number of photons in the energy interval k to k + dk striking this element of volume per standard BIP is

$$N(k)dk\; n(x,y)\, dxdy = U_o \frac{B(k/E_o, E_o)}{E_o k}\, dk\; n(x,y)\, dxdy \tag{4}$$

where n(x, y) is the spatial density of the beam at the target. The area over which n(x, y) is non-zero is determined by the beam collimators. This function is normalized so that

$$\int n(x,y)dxdy = 1 \tag{5}$$

where the integral is taken over the region in which n(x, y) is non-zero. The counting rate of the recoil protons from the π^o reaction that emerge from this volume at the angle θ_p^* within the solid angle $d\Omega$ and with momentum P^* is given by

$$dC = \frac{\rho N_o}{A} dz \quad \frac{d\sigma}{d\Omega'} \left(\frac{\partial \Omega'}{\partial \Omega}\right)_k d\Omega Q \quad \frac{B(k/E_o, E_o)}{k} dk \, n(x, y) \, dxdy \qquad (6)$$

where:

ρ is the density of the hydrogen

A is the atomic weight of hydrogen

$Q = U_o/E_o$ is the number of equivalent photons per standard BIP

N_o is Avogadro's number

$\frac{d\sigma}{d\Omega'}$ is the C.M. differential section for the π^o reaction

$\left(\frac{\partial \Omega'}{\partial \Omega}\right)_k$ is the ratio of C.M. differential solid angle to laboratory differential solid angle at a constant photon energy.

The relationship between k, θ_p^* and P^* is given by the formula

$$k = \frac{\frac{1}{2}(m^2 - 2M^2) + M\sqrt{P^{*2} + M^2}}{M + P^* \cos\theta_p^* - \sqrt{P^{*2} + M^2}} \qquad (7)$$

where m and M are the mass of the π^o meson and the proton,

respectively. The solid angle ratio is given by the equation

$$\left(\frac{\partial\Omega'}{\partial\Omega}\right)_k = \frac{\beta^2(1-\beta_c^2)\left[(1-\beta\,\beta_c\cos\theta_p^*)^2 - (1-\beta^2)(1-\beta_c^2)\right]^{-\frac{1}{2}}}{(\beta - \beta_c\cos\theta_p^*)} \tag{8}$$

where

$$\beta = \frac{P^*}{\sqrt{P^{*2} + M^2}} \tag{9}$$

and

$$\beta_c = \frac{k}{k+M} \tag{10}$$

In order to take account of the loss of counts due to effects such as nuclear absorption and coulomb scattering in the scintillation counters, equation 6 must be multiplied by a correction factor R. The total counting rate observed by the detection system is then

$$C = \frac{\rho N_o}{A} R \int \frac{d\sigma}{d\Omega'}\left(\frac{\partial\Omega'}{\partial\Omega}\right)_k d\Omega\, Q\, \frac{B(k/E_o, E_o)}{k}\, dk\, n(x,y)\, dxdydz \tag{11}$$

The limits of x and y have already been discussed. The limits of z depend on x and y and the dimensions of the target. The limits on k and Ω are determined by the magnetic spectrometer-scintillation counter system and in general depend on x, y and z. Since the only unknown quantity in the integrand is $\frac{d\sigma}{d\Omega'}$, equation 11 is written as

$$C = \frac{\rho N_o}{A} R \sigma(\bar{k}, \bar{\theta}'_\pi) \int \left(\frac{\partial \Omega'}{\partial \Omega}\right)_k d\Omega \frac{Q B(k/E_o, E_o)}{k} dk\, n(x, y)\, dxdydz \quad (12)$$

where

$$\sigma(\bar{k}, \bar{\theta}'_\pi) = \frac{\int \frac{d\sigma}{d\Omega'} \left(\frac{\partial \Omega'}{\partial \Omega}\right)_k \frac{B(k/E_o, E_o)}{k} n(x, y)\, d\Omega\, dkdxdydz}{\int \left(\frac{\partial \Omega'}{\partial \Omega}\right)_k \frac{B(k/E_o, E_o)}{k} n(x, y)\, d\Omega dkdxdydz} \quad (13)$$

Here $\bar{k}$ and $\bar{\theta}'_\pi$ represent central values of the k and θ'_π resolution functions which will be discussed later. The bar over the variables will be dropped in later sections for convenience of writing.

Because the protons experience energy loss in penetrating the hydrogen, the Mylar cup, the radiation shields, the external target window and the air path, they enter the magnet with a lower momentum P. Let all this material expressed in terms of its equivalent hydrogen range be denoted by Δr. This quantity depends on the point in the target where the protons are produced. If P^* is expressed in terms of its hydrogen range by the equation

$$P^* = f(r) \quad (14)$$

then P is given by

$$P = f(r - \Delta r) \quad (15)$$

To see more clearly the effect of energy loss, a transformation of variables from k to P will be made by substituting into the integral

of equation 12 the relation

$$dk = \left(\frac{\partial k}{\partial P^*}\right)_{\theta_p^*} \frac{\partial P^*}{\partial P} \, dP \tag{16}$$

where

$$\left(\frac{\partial k}{\partial P^*}\right)_{\theta_p^*} = \beta \, \frac{M + k\,(1 - 1/\beta \cos \theta_p^*)}{M + P^* \cos \theta_p^* - \sqrt{P^{*2} + M^2}} \tag{17}$$

and

$$\frac{\partial P^*}{\partial P} = \frac{f'(r)}{f'(r - \Delta r)} \tag{18}$$

Equation 12 is then written

$$C = \frac{\rho N_o}{A} \, R \, Q \, \sigma(\bar{k}, \bar{\theta}'_\pi) \int \left[\left(\frac{\partial \Omega'}{\partial \Omega}\right)_k \left(\frac{\partial k}{\partial P^*}\right)_{\theta_p^*} \frac{B(k/E_o, E_o)}{k} \, n(x, y) \right.$$

$$\left. \frac{f'(r)}{f'(r - \Delta r)} \, dP d\Omega \, dx dy dz \right] \tag{19}$$

If the energy loss is very small in comparison to the energy of the protons, $\Delta r/r$ is very small and the f' ratio in the integrand can be set equal to unity. If the dependence of the limits of Ω and P on the target variables can be neglected, the integration over target variables can be performed easily to obtain the factor

$$\int n(x, y)\, dxdydz = \bar{\ell} \qquad (20)$$

which is generally referred to as the effective length of the target. With the collimators used during this experiment $\bar{\ell}$ was 7 cm. For many of the runs made in this experiment $\Delta r/r$ was large enough so that the integrand of equation 19 became a function of the target variables which had too large a variation over the target to neglect.

Since the integral in equation 12 is quite complex, it was calculated numerically on the Cal Tech Electrodata digital computer. The computer program for the medium-high momentum magnet was coded by P. L. Donoho and the details are given elsewhere (14). In order to see what the k resolution function for a given angle and momentum setting of the magnetic spectrometer-scintillation counter system is, the computer is made to print out the function

$$K(k) = \int \left(\frac{\partial \Omega'}{\partial \Omega}\right)_k \frac{B(k/E_o, E_o)}{k}\, n(x, y)\, d\Omega\, dxdydz \qquad (21)$$

The quantity $K(k)/K_{max}$ is plotted in figure 8 for some typical medium and high momentum magnet runs. The central value of k for most of the runs was 490, 585, 690, 785 and 940 Mev. For any one of these energies the resolution function, whether the point was taken with the medium or high momentum magnet, is practically identical to the one shown in figure 8.

For the low momentum magnet runs it was necessary to take into account the effects of scattering in the hydrogen target. When

Figure 8. Energy Resolution for Medium and High Momentum Magnets.

The figure shows the photon energy resolution provided by the magnets when the π^o reaction is studied. The value of k which divides each resolution function into equal areas is referred to as the central value of k. Both magnets provide essentially the same resolution and this resolution is practically independent of the angle setting of the magnet provided the central k value remains the same. The curves have central values of k = 490, 585, 690, 785, 940 Mev. Most of the data have k values very close to these (see Table II).

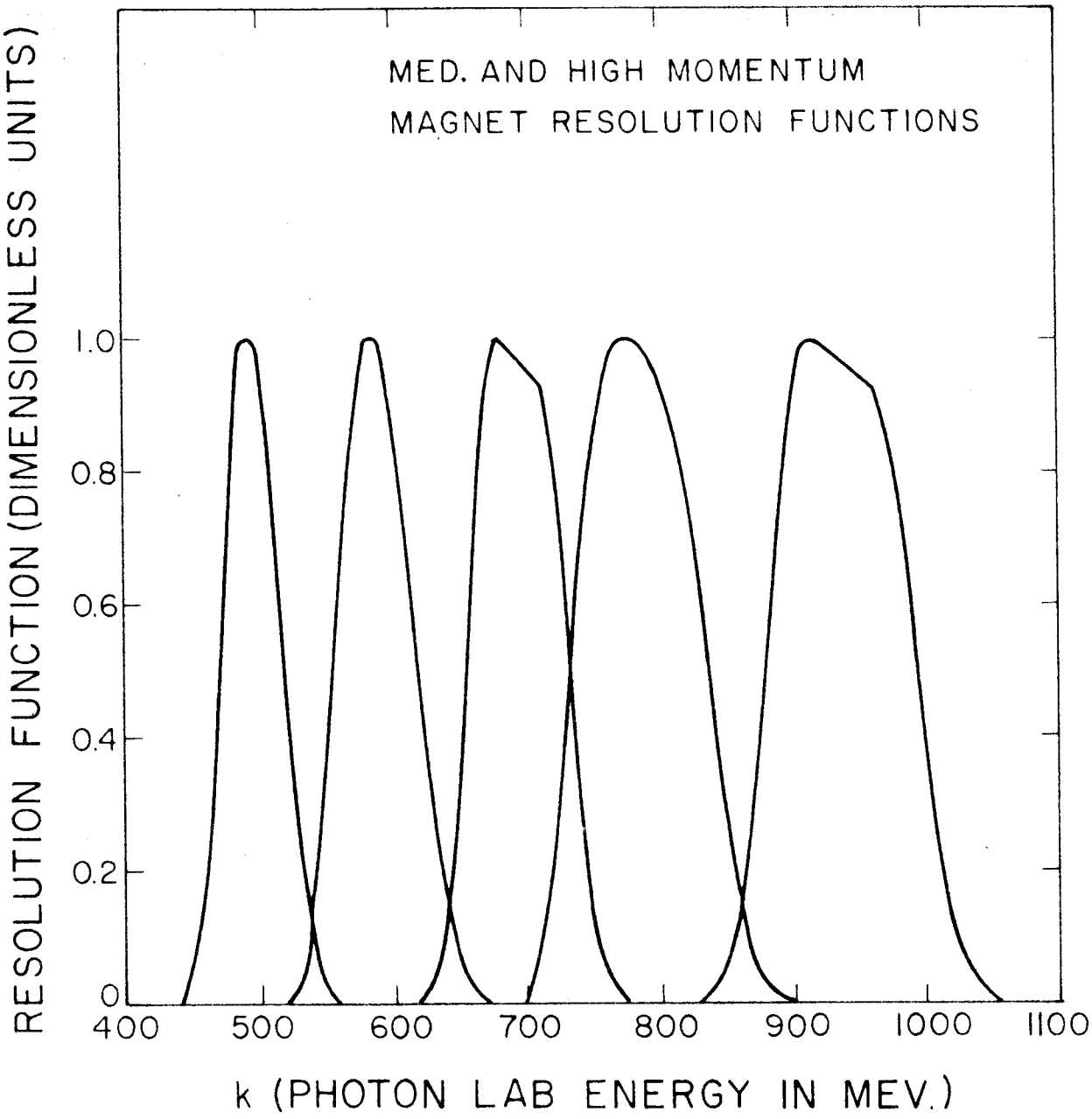
MED. AND HIGH MOMENTUM
MAGNET RESOLUTION FUNCTIONS
RESOLUTION FUNCTION (DIMENSIONLESS UNITS)
1.0
0.8
0.6
0.4
0.2
0
400
500
600
700
800
900
1000
1100
k (PHOTON LAB ENERGY IN MEV.)

scattering is considered, there is a distinction between the angle of production, θ_p^*, and the angle, θ_p, with which the proton leaves the target. Equation 11 must be changed to the following formula

$$C = \frac{\rho N_o}{A} R \int \left[\frac{d\sigma}{d\Omega'} \left(\frac{\partial \Omega'}{\partial \Omega} \right)_k d\Omega \, Q \, \frac{B(k/E_o, E_o)}{k} \, dk \right.$$

$$\left. n(x, y)\, dx dy dz \; P(\Omega \rightarrow \Omega_1)\, d\Omega_1 \right] \qquad (22)$$

where $P(\Omega \rightarrow \Omega_1)$ is the probability that a proton is scattered from the solid angle $d\Omega$ at Ω into the solid angle $d\Omega_1$ at Ω_1. In this case the detection system determines the limits of Ω_1 rather than Ω. Two types of scattering were considered, small angle multiple Coulomb scattering and single wide angle nuclear scattering events.

The rms Coulomb scattering angle was only the order of 1^o, but the quantity $\frac{\partial k}{\partial \theta_p^*}$ was approximately 70 Mev./degree in the region where the low momentum magnet was used. Consequently this small scattering angle was enough to spread the photon resolution function over the top of the bremsstrahlung resulting in a lower value for the integral than would be obtained if it were evaluated without scattering. Essentially the angular distribution of protons in the target at these lab angles (63^o - 70^o) is so sharply cut off by the bremsstrahlung limit that scattering in the target results in more particles being scattered out of the detection system than are scattered into it.

The probability that a proton, in passing out of the target, would undergo nuclear scattering was 1 - 2 ^{o}/o in the momentum range 200 - 275 Mev./c. It was not apparent that scattering in would be compensated by scattering out for this type of scattering. The π^{o} cross section in the region above 600 Mev. is down from the value around the resonance by a factor of about 10. Protons produced by photons around the resonance energy at more forward angles could undergo a wide angle scattering event which would result in a proton having the proper momentum and direction to be counted by the detection system. For these reasons it was necessary to consider quantitatively the effect of nuclear scattering.

The complete scattering problem was treated in the following manner. The function $P(\Omega \rightarrow \Omega_1)$ was broken into two parts

$$P(\Omega \rightarrow \Omega_1) \approx P_n(P^*, \Delta r)\, P_c(\Omega \rightarrow \Omega_1) + P_n(\Omega \rightarrow \Omega_1) \qquad (23)$$

where $P_n(P^*, \Delta r)$ is the probability that no nuclear scattering occurs, $P_c(\Omega \rightarrow \Omega_1)$ *is the probability that protons scatter from* Ω to Ω_1 by small angle multiple Coulomb scattering (19) and $P_n(\Omega \rightarrow \Omega_1)$ is the probability that protons scatter from Ω to Ω_1 by nuclear scattering (20, 21). This method neglects the interference between Coulomb and nuclear scattering plus the effects of multiple scattering after a nuclear scattering event has occurred. However these will introduce very little error. A substitution of equation 23 into equation 22 gives

$$C = \rho N_o \frac{R}{A} Q \left\{ \sigma(\bar{k}, \bar{\theta}_\pi') \int \left[\left(\frac{\partial \Omega'}{\partial \Omega} \right)_k d\Omega \frac{B(k/E_o, E_o)}{k} n(x, y) \right. \right.$$

$$\left. dk dx dy dz \, P_n \, P_c (\Omega \rightarrow \Omega_1) \, d\Omega_1 \right]$$

$$+ \int \left[\frac{d\sigma}{d\Omega'} \left(\frac{\partial \Omega'}{\partial \Omega} \right)_k d\Omega \frac{B(k/E_o, E_o)}{k} n(x, y) \right.$$

$$\left. \left. dk dx dy dz \, P_n (\Omega \rightarrow \Omega_1) \, d\Omega_1 \right] \right\} \qquad (24)$$

Both of these integrals were done on the Electrodata computer with programs coded by J. I. Vette. The specific details of the programs are given elsewhere (13). In the second integral of equation 24, $\frac{d\sigma}{d\Omega'}$ was evaluated by the data of Oakley and Walker (4) for photon energies below 450 Mev.; the contributions above 450 Mev. were negligible. This second term was treated as a contamination rate since it arises from protons produced in hydrogen which were not desired. This contamination rate was 1 - 2 $^o/o$ of the true counting rate. The computer program to do the first integral makes the computer print out

$$K(k) = \int \left(\frac{\partial \Omega'}{\partial \Omega} \right)_k d\Omega \frac{B(k/E_o, E_o)}{k} n(x, y) \, P_n \, P(\Omega \rightarrow \Omega_1) \, dx dy dz d\Omega_1 \qquad (25)$$

Two plots of $K(k)/K_{max}$ for the low momentum magnet are given in figure 9; a comparison with figure 8 shows that the resolution for the low momentum points is much poorer than the rest.

Figure 9. Energy Resolution for Low Momentum Magnet.

The figure shows the photon energy resolution for two of points studied with the low momentum magnet. The curve with an 880 Mev. central value corresponds to a magnet angle of 70° and a 261 Mev./c central momentum. The curve with the central value of 584 Mev. corresponds to a magnet setting of 63.5° and 250 Mev./c. The effects of scattering in the target have been included in the calculation. The fact that $\frac{\partial k}{\partial P}$ and $\frac{\partial k}{\partial \theta}$ are large in this region results in much wider resolution functions than those shown in figure 8.

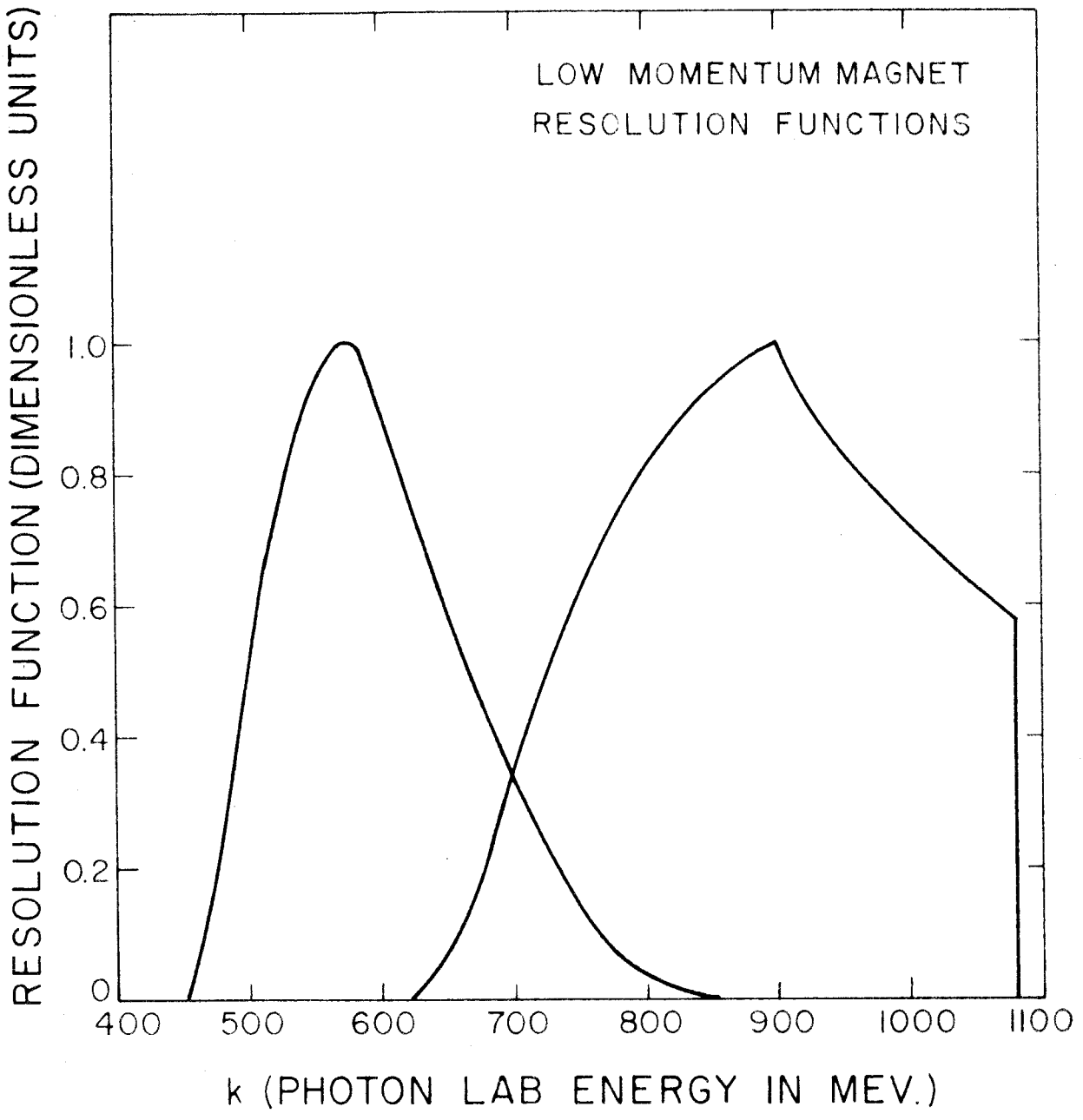
LOW MOMENTUM MAGNET
RESOLUTION FUNCTIONS
RESOLUTION FUNCTION (DIMENSIONLESS UNITS)
1.0
0.8
0.6
0.4
0.2
0
400
500
600
700
800
900
1000
1100
k (PHOTON LAB ENERGY IN MEV.)

The values m = 135.1 Mev. and M = 938.2 Mev. were used in all the calculations discussed in this section. The material in the target plus any air path was converted to its equivalent hydrogen range by the tables of Rich and Madey (22) and the relation between momentum and its range in hydrogen was also obtained from these tables. The density of the hydrogen in the target was 0.0726 gm/cc. (23). The correction factor R will be discussed in the next section. Once all these calculations are made, the average C.M. differential cross section can be obtained by

$$\sigma(\bar{k}, \bar{\theta}'_{\pi}) = \mathcal{K} C \tag{26}$$

where

$$\frac{1}{\mathcal{K}} = \rho N_o \frac{R}{A} \Omega \int K(k)\, dk \tag{27}$$

VI. CORRECTIONS

There were a number of corrections applied to the data before the cross sections were computed. These corrections can be divided into two groups; one constitutes the multiplicative factor R mentioned in the previous section. The other arises from protons produced in hydrogen by reactions other than the one under investigation. The counting rate from these undesired reactions is referred to as a contamination rate. The factor R will be discussed first.

The rear counter that was used with the medium momentum magnet was not quite large enough to catch all particles passing through the central counter. This reduced the momentum acceptance interval to 96.5 °/o of the value obtained by the stretched wire measurements. This same rear counter caused a reduction in the solid angle of 2.8 °/o when it was used with the high momentum magnet. A calculation of the Coulomb scattering in the counters gave a negligible correction. Nuclear absorption in the counters was measured by narrowing down the central counter with a lead slit to be certain that all particles passing through this counter from the magnet would strike the rear counter. Then the ratio of 1.2 to 1.2.3 coincidences was measured. The absorption cross section obtained in this manner was slightly less than the geometric cross section. The correction for this effect varied from 0 for the low momentum magnet runs up to 4.4 °/o.

Most of the high momentum magnet runs were made with a 1/2 inch piece of lead between the first and second counter to reduce

the background counts which did not come through the magnet. The absorption for this lead was measured by placing it directly in front of the rear counter and comparing the 1.2 and 1.2.3 coincidences. After taking account of the absorption in the central counter, this correction was found to be 8 °/o. Both the absorption cross section for the lead and the counter were shown to be independent of the momentum of the protons in the region of interest. The loss of counts due to the scattering of protons in the lead was calculated by Dr. R. L. Walker and was measured. The calculated correction was a little smaller than the measured one; an average of these two was used as the correction since both methods were susceptible to error. This momentum dependent correction varied from 0 - 3 °/o. All of the above factors were combined to make the total correction factor R.

The small source of undesired protons for the low momentum runs coming from the π^o reaction has been discussed in the previous section. These protons are not desired because they come from photons of lower energy than the region under investigation. The second reaction that can contribute to the contamination rate is Compton scattering. Measurements of this process up to photon energies of 270 Mev. (24) show that this cross section is about 1 °/o of the π^o cross section at the same energies. Mathews (12) has calculated the Compton cross section up to 270 Mev. by the use of dispersion theory. This type of calculation shows there is a relationship between these two processes. It is doubtful that the Compton cross section is ever more than several percent of the π^o cross

section at the same photon energy (25). Figure 10 shows the similarity of the dynamics of these reactions in the region in which this experiment is concerned. Because of these considerations, no correction for this process was made.

The contamination of protons coming from the production of meson pairs was briefly discussed in Section IV. Since this reaction contributes an appreciable fraction of the protons that are detected at the forward lab angles, the correction for this effect will be discussed in some detail. In the region where this correction is necessary, protons have a large enough momentum that energy loss in the target can be neglected.

The proton counting rate per standard BIP due to the pair production of mesons is

$$C_1 = \rho N_o \bar{\ell} \frac{R}{A} \Omega \int \frac{d^2\sigma}{dE' d\Omega'} \frac{B(k/E_o, E_o)}{k} dE' dk d\Omega' \qquad (1)$$

Where E' is the total C.M. energy of the proton. The quantity

$$\sigma_1(k) = \int \frac{d^2\sigma}{dE' d\Omega'} dE' d\Omega' \qquad (2)$$

is the total cross section for pair production at photon energy k. Here the integration extends over the full range of the variables. Since the detection system provides limits for the laboratory solid angle, it is convenient to make the solid angle transformation from C.M. to lab system. Then

Figure 10. Kinematics for Compton Scattering and π^o Photoproduction.

The solid curves give the proton laboratory momentum versus laboratory angle at constant photon energies for the $\gamma + P \longrightarrow \pi^o + P$ reaction. The dotted curves give the same kinematics for the $\gamma + P \longrightarrow \gamma' + P$ reaction.

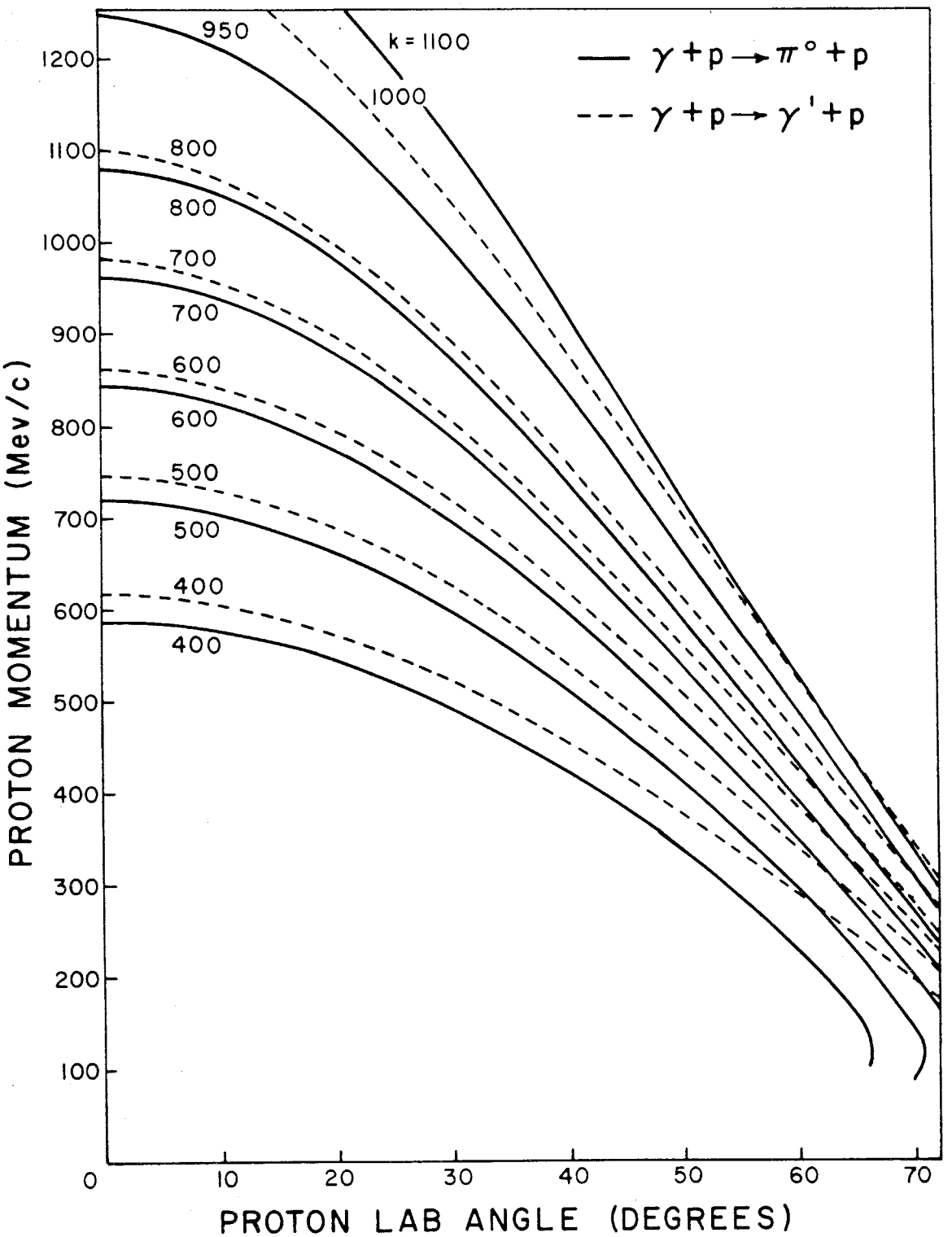
950
k = 1100
1000
800
800
700
700
600
600
500
500
400
400
γ + p → π° + p
γ + p → γ' + p
PROTON MOMENTUM (Mev/c)
PROTON LAB ANGLE (DEGREES)
0
100
200
300
400
500
600
700
800
900
1000
1100
1200
10
20
30
40
50
60
70

$$C_1 = D \int \frac{d^2\sigma}{dE'd\Omega'} \left(\frac{\partial \Omega'}{\partial \Omega}\right)_{k,E'} \frac{B(k/E_o, E_o)}{k} \, dE' dk \, d\Omega \quad (3)$$

where $D = \rho N_o \frac{R}{A} Q$. The quantity $\left(\frac{\partial \Omega'}{\partial \Omega}\right)_{k,E'}$ is given by equation VI-8, but there is now no unique relation between k, θ_p^* and P^* since pair production involves three particles in the final state. After the change of variables from E' to P is made, equation 3 becomes

$$C_1 = D \int \frac{d^2\sigma}{dE'd\Omega'} \left(\frac{\partial \Omega'}{\partial \Omega}\right)_{k,E'} \left(\frac{\partial E'}{\partial P}\right)_{\theta_p^* k} \frac{B(k/E_o, E_o)}{k} \, dP \, dk \, d\Omega \quad (4)$$

where

$$\left(\frac{\partial E'}{\partial P}\right)_{\theta_p^*, k} = \frac{\beta - \beta_c \cos \theta_p^*}{\sqrt{1 - \beta_c^2}} \quad (5)$$

In order to proceed further it is necessary to obtain some expression for $\frac{d^2\sigma}{dE'd\Omega'}$.

Protons arise from photomeson pair production in hydrogen by the two reactions:

$$\gamma + P \longrightarrow \pi^o + \pi^o + P \quad (6)$$

$$\gamma + P \longrightarrow \pi^+ + \pi^- + P \quad (7)$$

At energies well above threshold (k = 320), it might be expected

that the two reactions would be comparable since the production of single neutral and charged mesons is similar for energies well above threshold. Bloch and Sands (11) have obtained $\frac{d^2\sigma_c}{dE'_{\pi^-} d\Omega'_{\pi^-}}$ for reaction 7 by subtracting the yields of π^- measured from hydrogen at different values of E_o, the maximum energy of the bremsstrahlung. Their measurements indicate that this quantity is roughly isotropic in the C.M. system and the energy dependence on E'_{π^-}, the C.M. total energy of the π^-, is not inconsistent with a density of states factor obtained by integrating out the proton and positive meson variables from a three particle final state density.

With these facts in mind, the cross section is divided into the contributions from reaction 6 and 7; then it is assumed that the cross section for reaction 6 is proportional to that of 7. Thus

$$\frac{d^2\sigma}{dE' d\Omega'} = (1 + a) \frac{d^2\sigma_c}{dE' d\Omega'} \tag{8}$$

where a is the proportionality factor mentioned above. In analogy with the information obtained by Bloch and Sands, it is assumed that the cross section can be written

$$\frac{d^2\sigma_c}{dE' d\Omega'} = \left|L(k)\right|^2 g(k, E') \tag{9}$$

where $g(k, E')$ is obtained by integrating out the meson variables from a three particle density of states. Berman (26) has obtained the

formula

$$g(k, E') = \pi E' \left[(W - E') \ (E_+^2 - E_-^2) \ - \ \frac{2}{3} \ (E_+^3 - E_-^3) \right] \tag{10}$$

where

$$W \ = \ M \sqrt{1 + 2k/M} \tag{11}$$

and

$$E_{\pm} = \frac{(W-E') \ \pm \sqrt{(W-E')^2 - (W^2+M^2-2E'W) + \frac{4m^2(E'^2-M^2)}{(W^2+M^2-2E'W)}}}{2} \tag{12}$$

It is possible to evaluate $\left|L(k)\right|^2$ by the data of Bloch and Sands. An integration of equation 9 yields

$$\int \frac{d^2\sigma_c}{dE' d\Omega'} \ dE' d\Omega' = \sigma_c \ (k) = 4\pi \left|L(k)\right|^2 G(k) \tag{13}$$

where

$$G(k) \ = \int g(k, E')dE' \tag{14}$$

A smilar integration of the quantity measured by Bloch and Sands gives

$$\int \frac{d^2\sigma_c}{dE'_{\pi^-} d\Omega'_{\pi^-}} \ dE'_{\pi^-} d\Omega'_{\pi^-} \ = \ \sigma_c(k) = (4\pi) \ 4.5 \times 10^{-30} \text{cm}^2 \pm 30^o/o \tag{15}$$

essentially independent of k in the region between 600 and 980 Mev.

Using all this information equation 1 can be written

$$C_1 = \frac{(1+a)D}{4\pi}\int \sigma_c \frac{g(k,E')}{G(k)} \frac{\partial \Omega'}{\partial \Omega} \frac{\partial E'}{\partial P} \frac{B(k/E_o, E_o)}{k} dPdkd\Omega \qquad (16)$$

The evaluation of the integral in equation 16 was made numerically by J. I. Vette and Dr. R. L. Walker using the Electrodata computer. The dependence of the integrand on θ_p^* was neglected and the trivial integration over the solid angle performed before the numerical work was done.

In order to check the assumptions of this calculation and to evaluate the constant a, runs were made with different values of E_o while holding the magnet angle and momentum constant. This procedure changed the fraction of observed protons that came from meson pair production. Surprisingly these measurements, although they were very rough, indicated that $a = 0$ is not inconsistent. This will be shown in a moment.

The results of these calculations are presented in the following manner. The answer obtained from equation 16 with $a = 0$ was multiplied by κ (see equation V-27) to give a pseudo-π^o cross section which will be denoted by the symbol σ_p. This quantity is given in Table II in the next section.

The evidence that $a = 0$ and that the correction seems reasonable can be seen in figures 12 and 15 (see next section). The points denoted by the triangles were taken at a higher value of E_o than those denoted by the circles. It can be seen that after the pair correction is made, the two cross sections are within statistical errors.

Since the difference of the correction for a given point is large, the agreement of the final answer is a good indication that assumptions about $\frac{d^2\sigma_c}{dE'd\Omega'}$ are reasonable. If the data of Oakley and Walker (4) are extrapolated from 450 Mev. to 490 and 500 Mev., and compared with those two points in figures 12 and 15 which have just been discussed, the agreement is very good. Since these cross sections were computed on the basis of a pair correction with a = 0, and since these corrections were large, this value for a was used for all the corrections. It is possible that the method of calculation over-estimated the contribution from reaction 7; however with the data available reaction 6 seems small compared to 7. In general the pair correction is smaller than at these points where the calculation was checked.

VII. ERRORS AND EXCITATION FUNCTIONS

After the contamination and background rates were subtracted from C' to obtain C, the average C.M. differential cross sections were computed by the method discussed in Section V. The final results of the data reduction are given in Table II.

The errors have been classified into three types. The quoted errors are estimated standard errors.

A. Errors in the absolute cross section which are independent of the proton momentum and angle.

1. Beam calibration = $\pm$ 3 %.
2. Errors in K arising from errors in stretched wire measurements and in the dimensions of the target cup = $\pm$ 2 %.

B. Random statistical errors which vary from point to point.

1. Standard counting errors.
2. Small variations not accounted for by periodic monitoring.
   a. Ion chamber temperature = $\pm$ 1/2 %
   b. Peak energy of the synchrotron = $\pm$ 1/2 %.
3. Ion current integrator stability = $\pm$ 1.5 %.

C. Systematic errors which depend on the momentum, angle and E_o.

1. Error in nuclear absorption correction = $\pm$ 5 % of the correction.
2. Error in lead scattering correction = $\pm$ 20 % of the correction.
3. Error in the pair correction σ_p = $\pm$ 30 % of the correction.

TABLE II.

This table presents all the data obtained in this experiment. The magnet that was used to take the data is given in the first column. The central value of the pion C.M. angular resolution in degrees is given next. The third column lists the central value of the photon resolution in Mev. The average C.M. differential cross sections for the reaction $\gamma + P \longrightarrow \pi^o + P$ are in the fourth column. The B and C type errors are given in columns six and seven. The combination of these two statistical errors are given in the fifth column. The last column gives the calculated correction for the contamination of protons coming from meson pair production. This correction is expressed in terms of a pseudo-π^o cross section (see page 50). Without this correction the data would yield cross sections equal to the sum of the fourth and eighth columns.

Table II.

C.M. Differential Cross Sections in Units of 10^{-30} cm^2/ster.

Magnet	θ'_π	k	$\sigma(k, \theta'_\pi)$	B+C Error	Type B Error	Type C Error	σ_p
High	147	954	3.09	0.40	0.29	0.28	0.94
High	147	799	1.94	0.45	0.28	0.35	1.18
High	147	702	2.00	0.47	0.35	0.31	1.05
High	147	593	0.32	0.56	0.34	0.44	1.47
High	147	496	2.51	2.21	0.80	2.06	6.85
High	147	495	1.33	1.26	0.43	1.19	3.99
High	135	945	3.64	0.38	0.30	0.23	0.76
High	135	793	2.34	0.41	0.24	0.33	1.09
High	135	693	2.77	0.41	0.29	0.30	1.01
High	120	936	2.59	0.33	0.26	0.20	0.65
High	120	788	3.12	0.34	0.23	0.25	0.82
High	120	692	2.90	0.36	0.29	0.21	0.71
High	120	593	2.90	0.57	0.47	0.32	1.08
High	120	495	4.65	1.07	0.58	0.90	3.00
High	113	790	3.32	0.30	0.26	0.15	0.50
High	105	943	2.22	0.19	0.16	0.11	0.38
High	105	793	3.62	0.24	0.19	0.14	0.24
High	105	689	3.39	0.30	0.27	0.15	0.40
High	90	936	2.27	0.21	0.19	0.09	0.20
High	90	788	4.07	0.21	0.16	0.14	0.27
High	90	690	3.88	0.41	0.39	0.13	0.00
Med.	90	579	3.27	0.26	0.23	0.11	0.14
Med.	90	484	5.43	0.41	0.29	0.29	0.98
High	75	937	1.32	0.19	0.18	0.06	0.12
High	75	784	3.54	0.42	0.41	0.10	0.11
Med.	75	784	3.11	0.15	0.12	0.09	0.04
Med.	75	660	2.70	0.29	0.28	0.07	0.11
Med.	75	593	2.56	0.22	0.21	0.08	0.05
Med.	75	495	5.06	0.35	0.32	0.14	0.46
Med.	67.5	931	1.36	0.08	0.06	0.04	0.02
Med.	67.5	879	1.96	0.23	0.22	0.06	0.08
Med.	67.5	807	2.41	0.13	0.11	0.07	0.00
Med.	67.5	688	2.27	0.38	0.24	0.30	1.02
Med.	67.5	582	2.75	0.24	0.23	0.08	0.00
Med.	67.5	486	4.93	0.33	0.32	0.07	0.24
Med.	67.5	486	5.16	0.50	0.38	0.33	1.11
Med.	60	938	1.72	0.12	0.11	0.05	0.00
Med.	60	884	1.49	0.12	0.11	0.05	0.02
Med.	60	786	2.53	0.15	0.12	0.08	0.00

Table II. (Continued)

Magnet	θ_π'	k	$\sigma(k, \theta_\pi')$	B+C Error	Type B Error	Type C Error	σ_p
Med.	60	587	2.54	0.25	0.24	0.08	0.00
Med.	60	479	3.94	0.36	0.34	0.12	0.05
Med.	52.5	950	2.01	0.11	0.19	0.06	0.00
Med.	52.5	784	2.61	0.16	0.14	0.08	0.00
Med.	52.5	583	2.10	0.29	0.28	0.06	0.00
Med.	45	910	1.98	0.16	0.15	0.06	0.00
Med.	45	772	1.96	0.17	0.15	0.06	0.00
Low	45	640	1.69	0.27	0.26	0.07	0.10
Low	45	584	2.68	0.40	0.40	0.08	0.12
Low	45	524	3.96	0.35	0.34	0.11	0.12
Low	37	762	2.55	0.26	0.25	0.08	0.00
Low	37	734	2.37	0.26	0.26	0.07	0.00
Low	37	710	2.44	0.52	0.52	0.07	0.00
Low	37	680	2.12	0.43	0.42	0.06	0.00
Low	37	652	2.13	0.60	0.59	0.06	0.00
Low	37	620	2.42	0.31	0.30	0.07	0.00
Low	31.5	912	2.42	0.43	0.43	0.07	0.00
Low	31.5	880	3.21	0.28	0.26	0.10	0.00
Low	31.5	853	2.40	0.34	0.34	0.07	0.00
Low	31.5	825	2.46	0.35	0.35	0.07	0.00
Low	31.5	790	2.59	0.60	0.60	0.08	0.00
Low	31.5	760	2.52	0.64	0.64	0.08	0.00
Low	31.5	744	2.08	0.29	0.28	0.06	0.00

4. Error due to neglect of Compton scattering $< -3\%$.

5. Error due to aperture penetration = $\pm$ 0-1/2 %.

6. Error due to $\pm .05^{\circ}$ error in magnet angle and $\pm .1\%$ error in magnet momentum $< \pm 1/2\%$.

The excitation functions for various pion C.M. angles are plotted in figures 11-15.

Figures 11-15. Excitation Functions for Reaction $\gamma + P \rightarrow \pi^o + P$

The corrected C.M. differential cross sections (open circles) for a constant pion C.M. angle are plotted as a function of k. The errors are the combined B and C type errors defined on page 58. The solid points represent the correction calculated for the contribution of protons coming from meson pair production expressed in terms of a pseudo-π^o C.M. differential cross section. This correction does not necessarily show a smooth variation because it depends critically on the value of E_o which varied from point to point (see page 50). The values of θ'_π for each figure are given below.

Figure 11. $\theta'_\pi = 45^o$

Figure 12. $\theta'_\pi = 67.5^o$

The k = 490 Mev. data denoted by the triangle were taken with E_o = 1072 Mev. and the circle was taken with E_o = 722 Mev. Without the pair correction these two points would differ by more than the errors. An extrapolation of the Walker-Oakley data (7) from 450 to 490 Mev. gives

$\sigma(\theta'_\pi = 67.5^o) = 5 \times 10^{-30} cm^2/ster.$

Figure 13. $\theta'_\pi = 90^o$

Figure 14. $\theta'_\pi = 120^o$

Figure 15. $\theta'_\pi = 147^o$

The k = 500 Mev. point denoted by the triangle was taken with E_o = 946 Mev. and the circle was taken with E_o = 725 Mev. An extrapolation of the Walker-Oakley data from 450 to 500 Mev. gives

$\sigma(\theta'_\pi = 147^o) = 1.9 \times 10^{-30} cm^2/ster.$ Without the pair correction these two points would be very different and both would be too large.

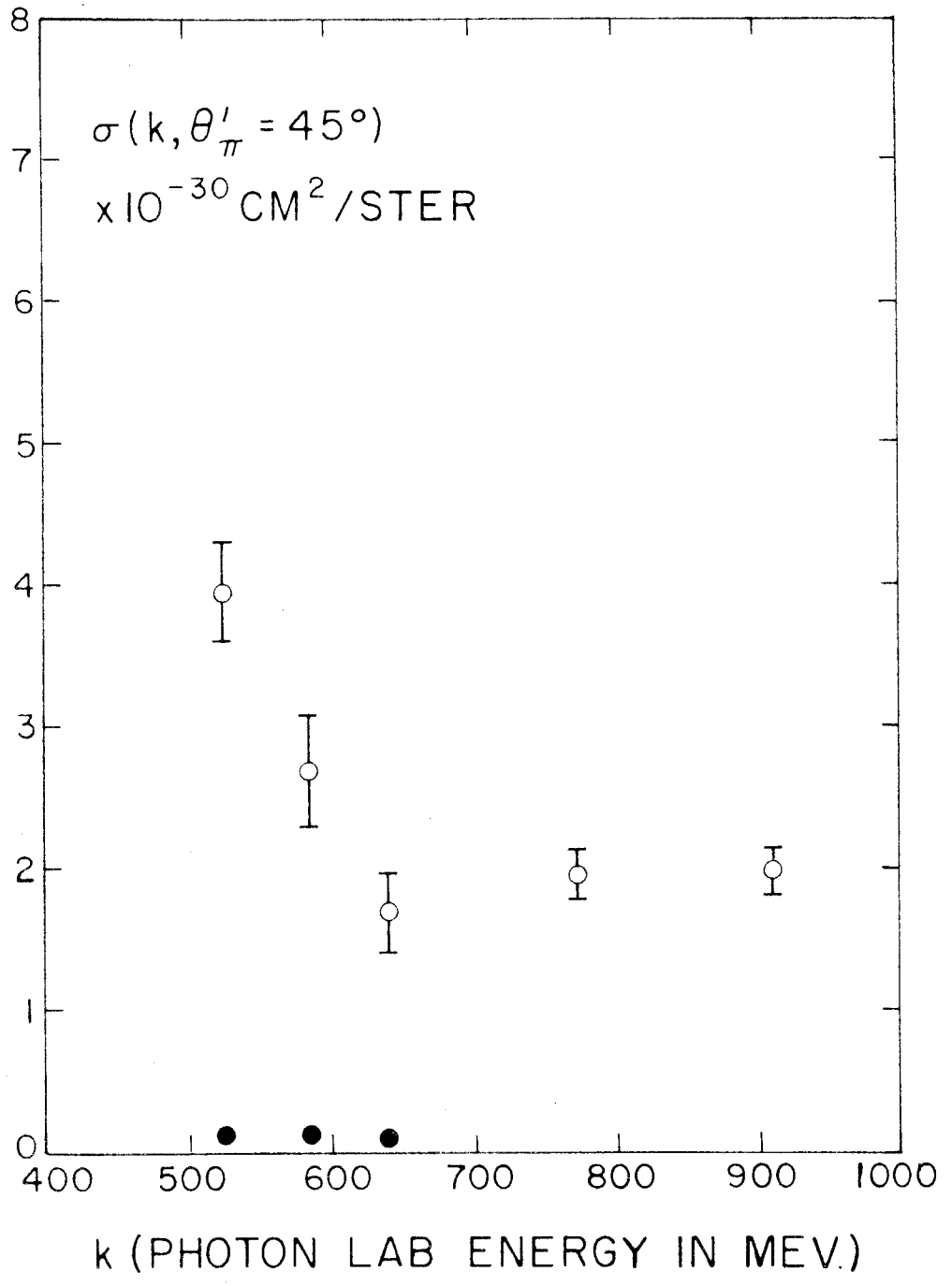
$\sigma(k, \theta'_\pi = 45°)$
$\times 10^{-30}$ CM^2/STER
8
7
6
5
4
3
2
1
0
400
500
600
700
800
900
1000
k (PHOTON LAB ENERGY IN MEV.)

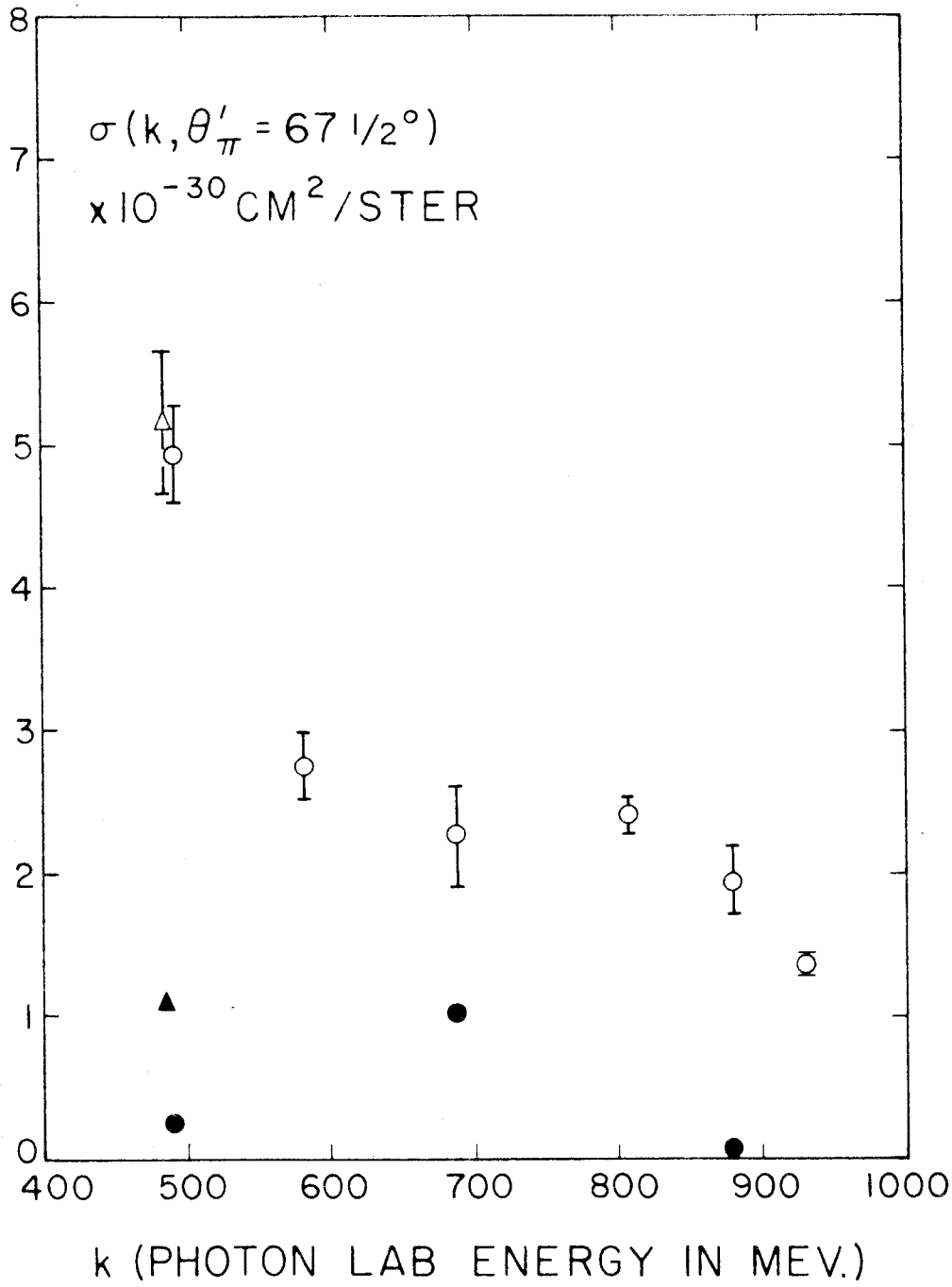
σ(k, θ'π = 67 1/2°)
x 10⁻³⁰ CM²/STER
8
7
6
5
4
3
2
1
0
400
500
600
700
800
900
1000
k (PHOTON LAB ENERGY IN MEV.)

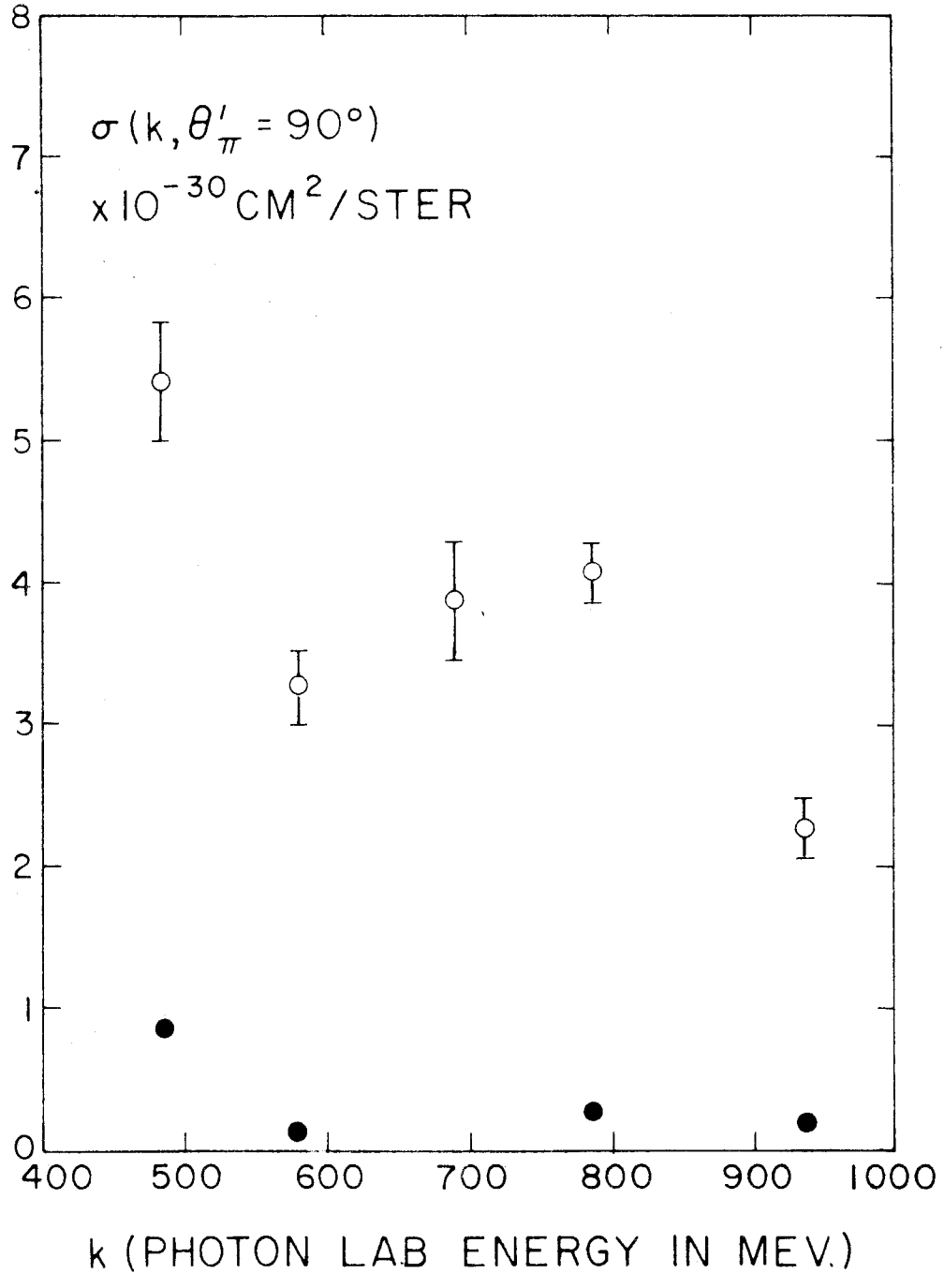
$\sigma(k, \theta'_\pi = 90°)$
$\times 10^{-30}$ CM^2/STER
8
7
6
5
4
3
2
1
0
400
500
600
700
800
900
1000
k (PHOTON LAB ENERGY IN MEV.)

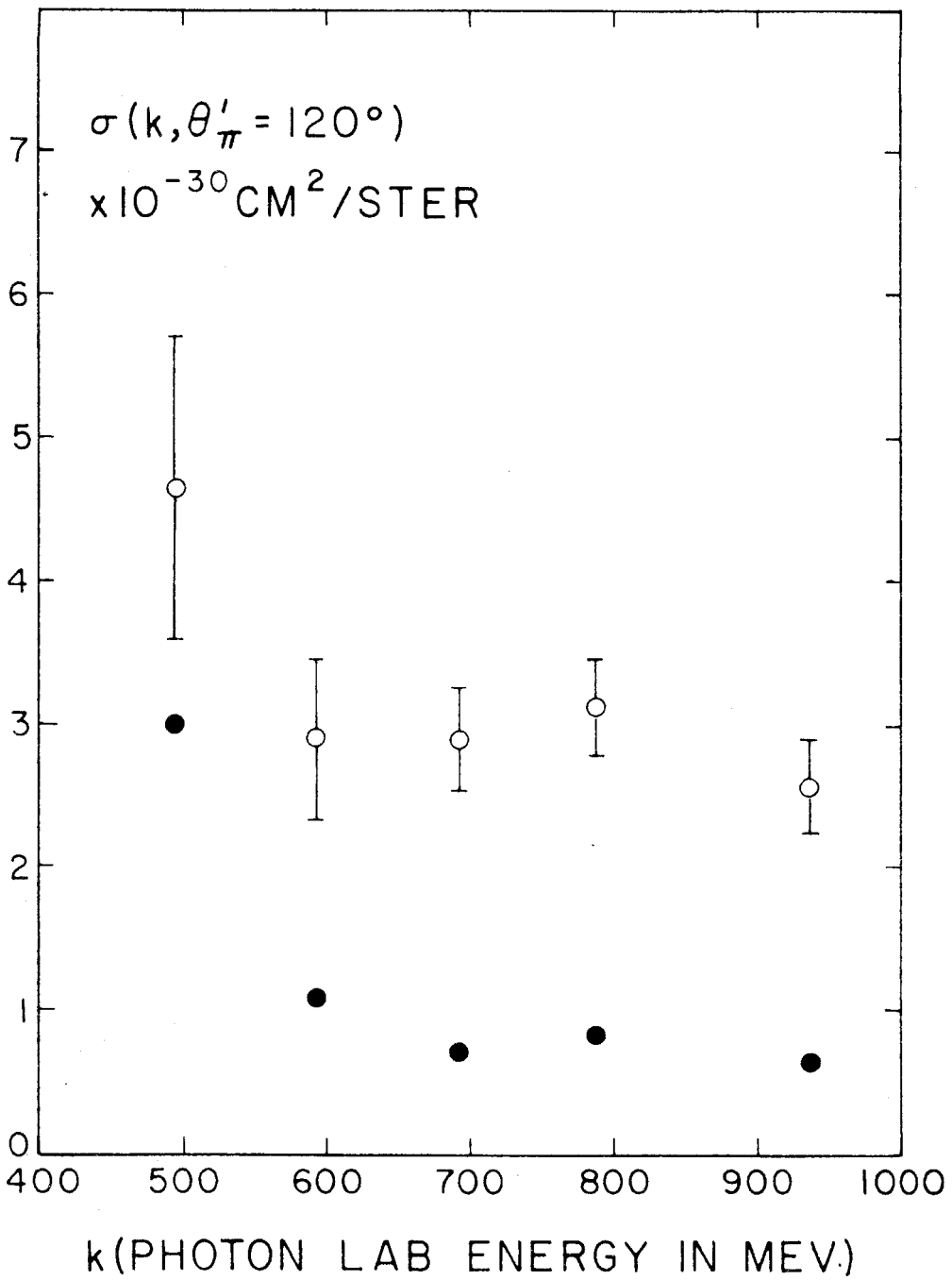
$\sigma(k, \theta'_\pi = 120°)$
$\times 10^{-30} CM^2/STER$
0
1
2
3
4
5
6
7
400
500
600
700
800
900
1000
k(PHOTON LAB ENERGY IN MEV.)

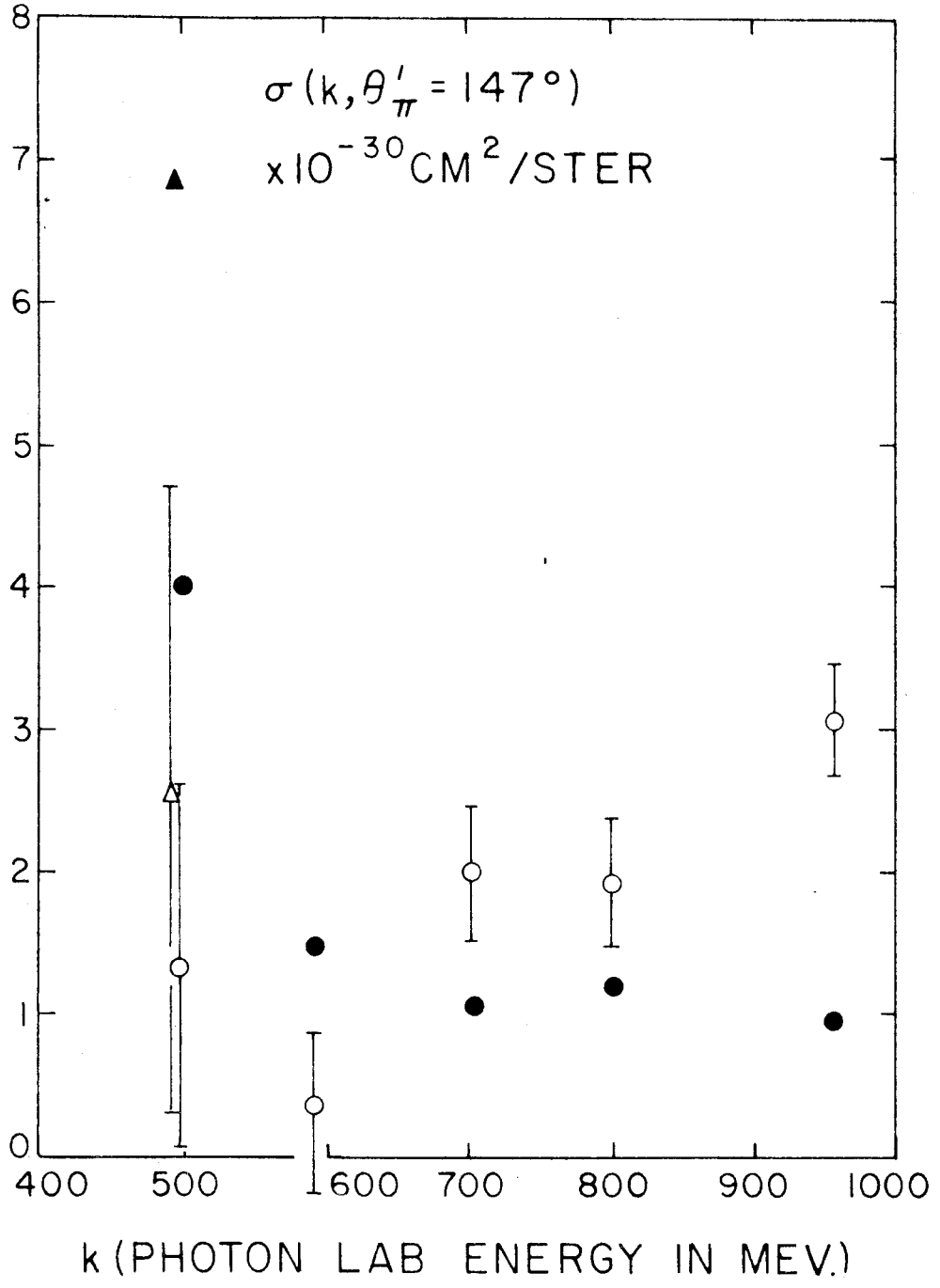
$\sigma(k, \theta'_\pi = 147°)$
$\times 10^{-30} CM^2/STER$
8
7
6
5
4
3
2
1
0
400
500
600
700
800
900
1000
k (PHOTON LAB ENERGY IN MEV.)

VIII. ANGULAR DISTRIBUTIONS

The angular distributions for the five energies investigated are plotted in figures 16-20. The C.M. angular resolutions are indicated at the bottom of each figure. The relationship between θ_π' and θ_p^* is given by the formula

$$\tan \theta_\pi' = - \frac{\sqrt{1 - \beta_c^2 \sin \theta_p^*}}{- \beta_c/\beta + \cos \theta_p^*} \qquad (1)$$

Figure 21 shows that the lines of constant θ_π' on a graph of P^* versus θ_p^* are nearly vertical in the region of investigation. In this case the angular resolution in the lab system is converted into one in the C.M. system by multiplying by a scale factor. Several of the values represented on the angular distributions were obtained by interpolating the excitation functions to the correct energy. However most of the points represent a direct measurement. For convenience the data plotted in figures 16-20 are listed in Table III.

Before beginning an analysis of the angular distribution it is desirable to make a few comments. The primary purpose of this experiment was to investigate the π^o reaction in the 700-950 Mev. region. However enough data were obtained at the lower energies to include in this report. The pair corrections for the 490 Mev. data were excessive because the data were taken with E_o = 720 Mev. It was not convenient to run with a lower value of E_o during the course of this experiment. There are not enough data backward of $\theta_\pi' = 90^o$ at the

Figures 16-20. Angular Distributions for Reaction $\gamma + P \longrightarrow \pi^o + P$

Each figure shows the C. M. differential cross sections for a constant photon laboratory energy plotted versus the pion C.M. angle. Most of the points represent a direct measurement; others are interpolations from the excitation functions. The errors are the combined B and C type errors defined on page 58. The angular resolutions are shown at the bottom of each figure. The solid and dotted curves are maximum likelihood (least squares) fits of the form

$$\sigma(\theta'_\pi, k) = \sum_{n=o}^{m} A_n(k) \cos^n \theta'_\pi$$

The value of m will be used to characterize each curve. The values of the photon energy and the identification of the fits are given below.

Figure 16. k = 490 Mev.

Solid curve is m = 2. Dotted curve is m = 3; this fit goes negative at 165° and as such is not acceptable.

Figure 17. k = 585 Mev.

Solid curve is m = 2. Dotted curve is m = 4; this fit goes negative at 150° and as such is not acceptable.

Figure 18. k = 690 Mev.

Solid curve is m = 2. Dotted curve is m = 4.

Figure 19. k = 785 Mev.

Solid curve is m = 2. Dotted curve is m = 4.

Figure 20. k = 940 Mev.

Solid curve is m = 2. Dotted curve is m = 4.

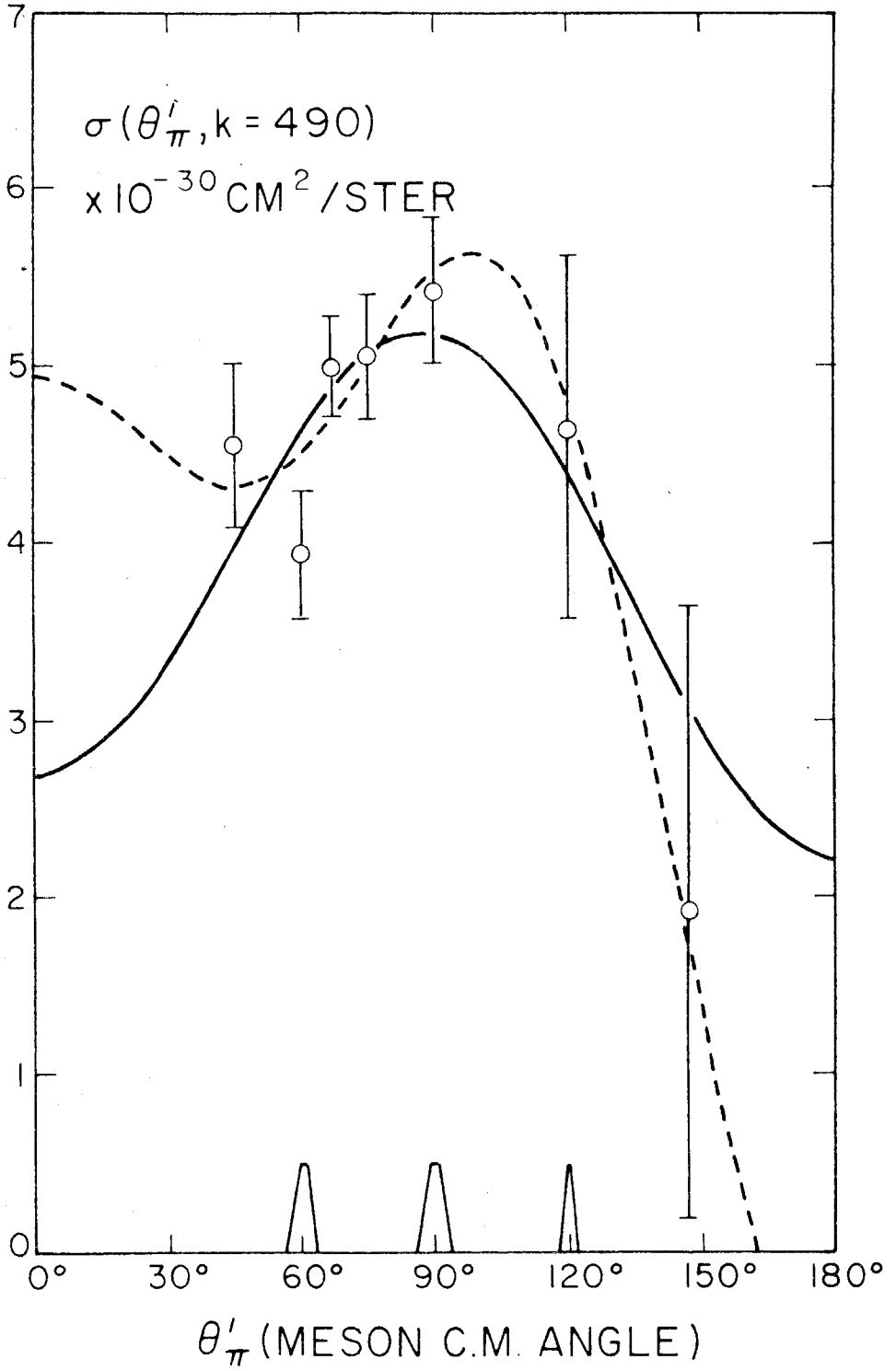
$\sigma(\theta'_\pi, k = 490)$
$\times 10^{-30}$ CM^2/STER
7
6
5
4
3
2
1
0
0°
30°
60°
90°
120°
150°
180°
θ'_π (MESON C.M. ANGLE)

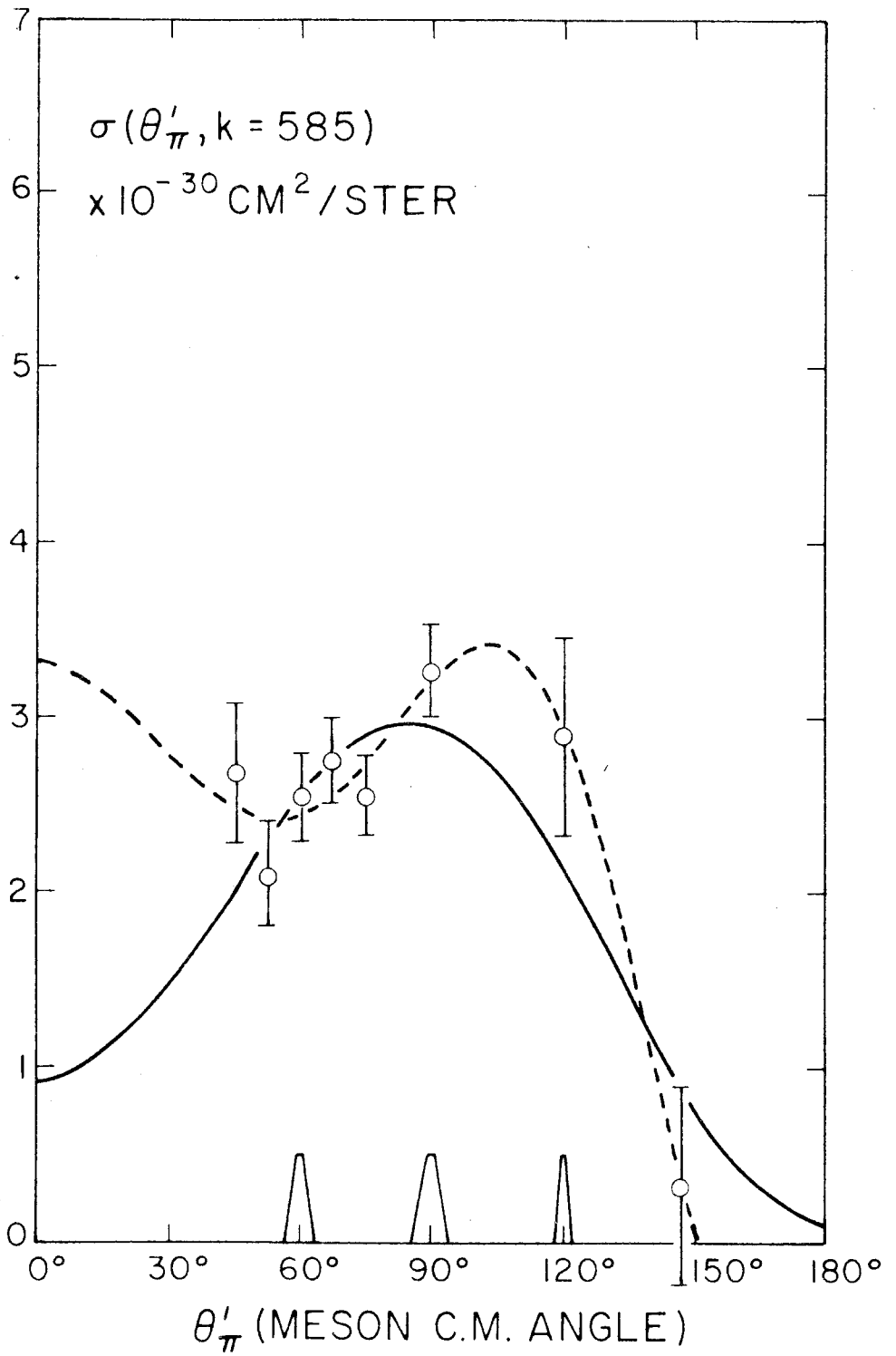
$\sigma(\theta'_\pi, k = 585)$
$\times 10^{-30}$ CM^2/STER
7
6
5
4
3
2
1
0
0°
30°
60°
90°
120°
150°
180°
θ'_π (MESON C.M. ANGLE)

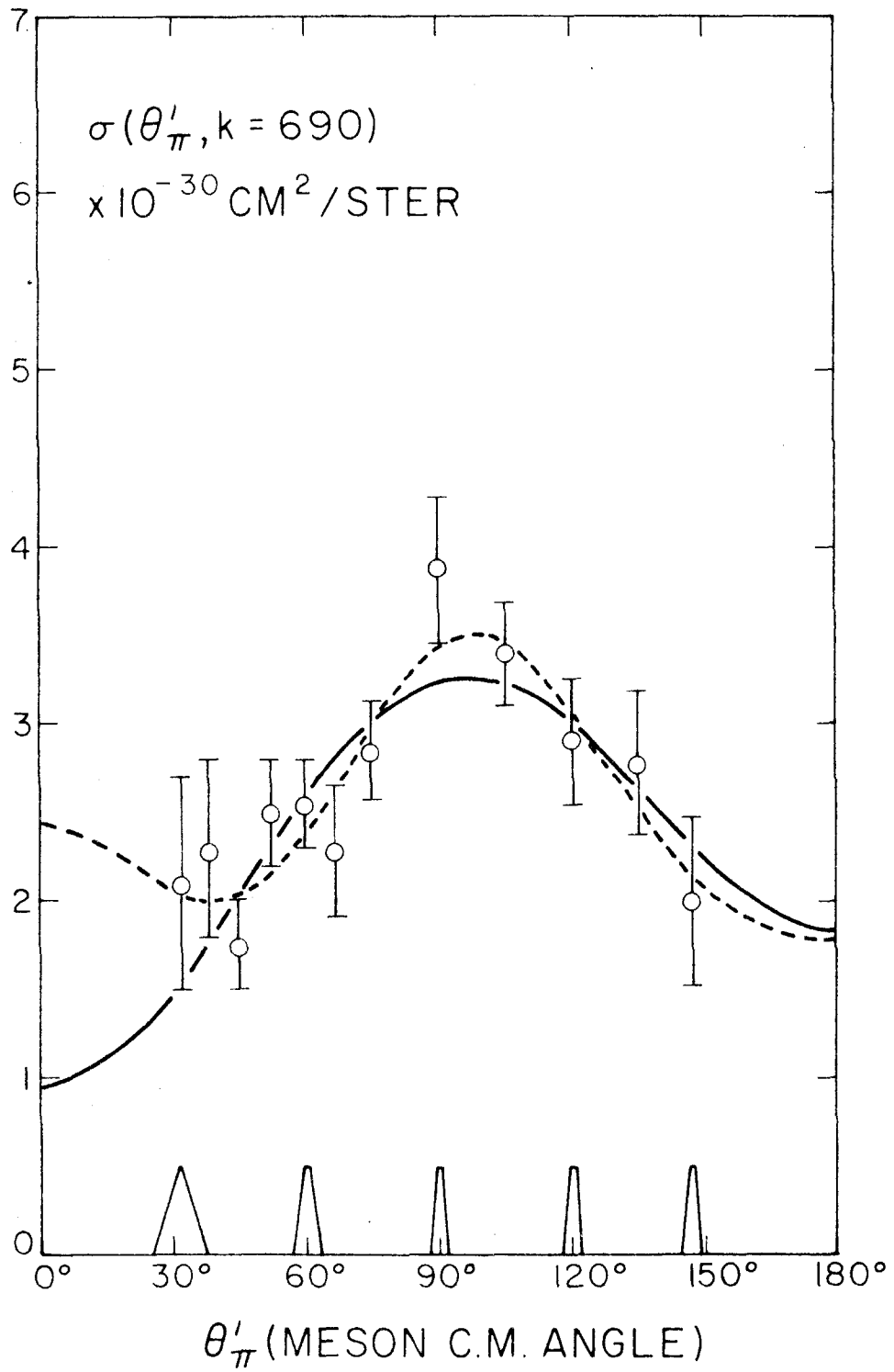
$\sigma(\theta'_\pi, k = 690)$
$\times 10^{-30}$ CM^2/STER
7
6
5
4
3
2
1
0
0°
30°
60°
90°
120°
150°
180°
θ'_π (MESON C.M. ANGLE)

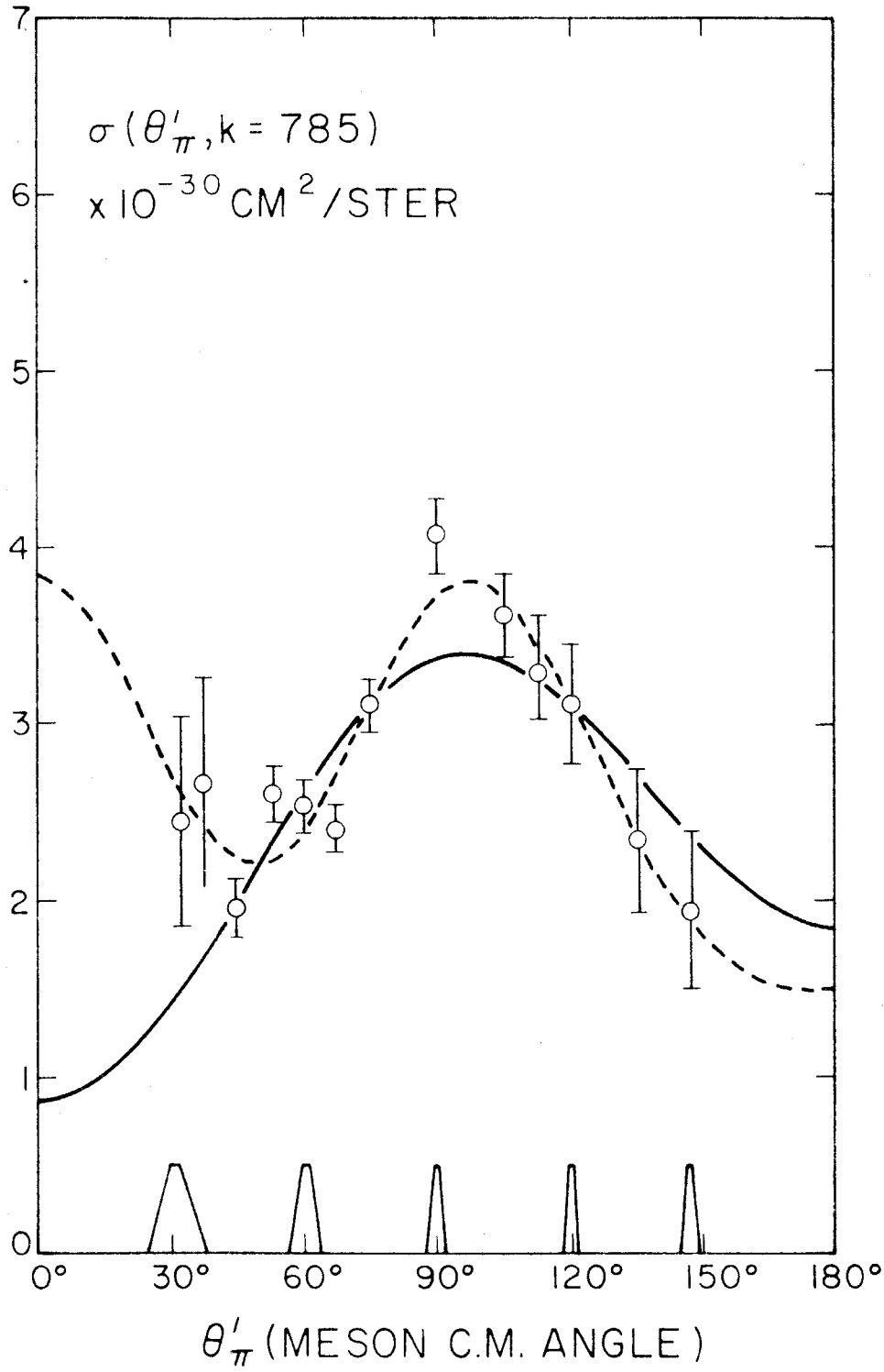
$\sigma(\theta'_\pi, k = 785)$
$\times 10^{-30}$ CM^2/STER
7
6
5
4
3
2
1
0
0°
30°
60°
90°
120°
150°
180°
θ'_π (MESON C.M. ANGLE)

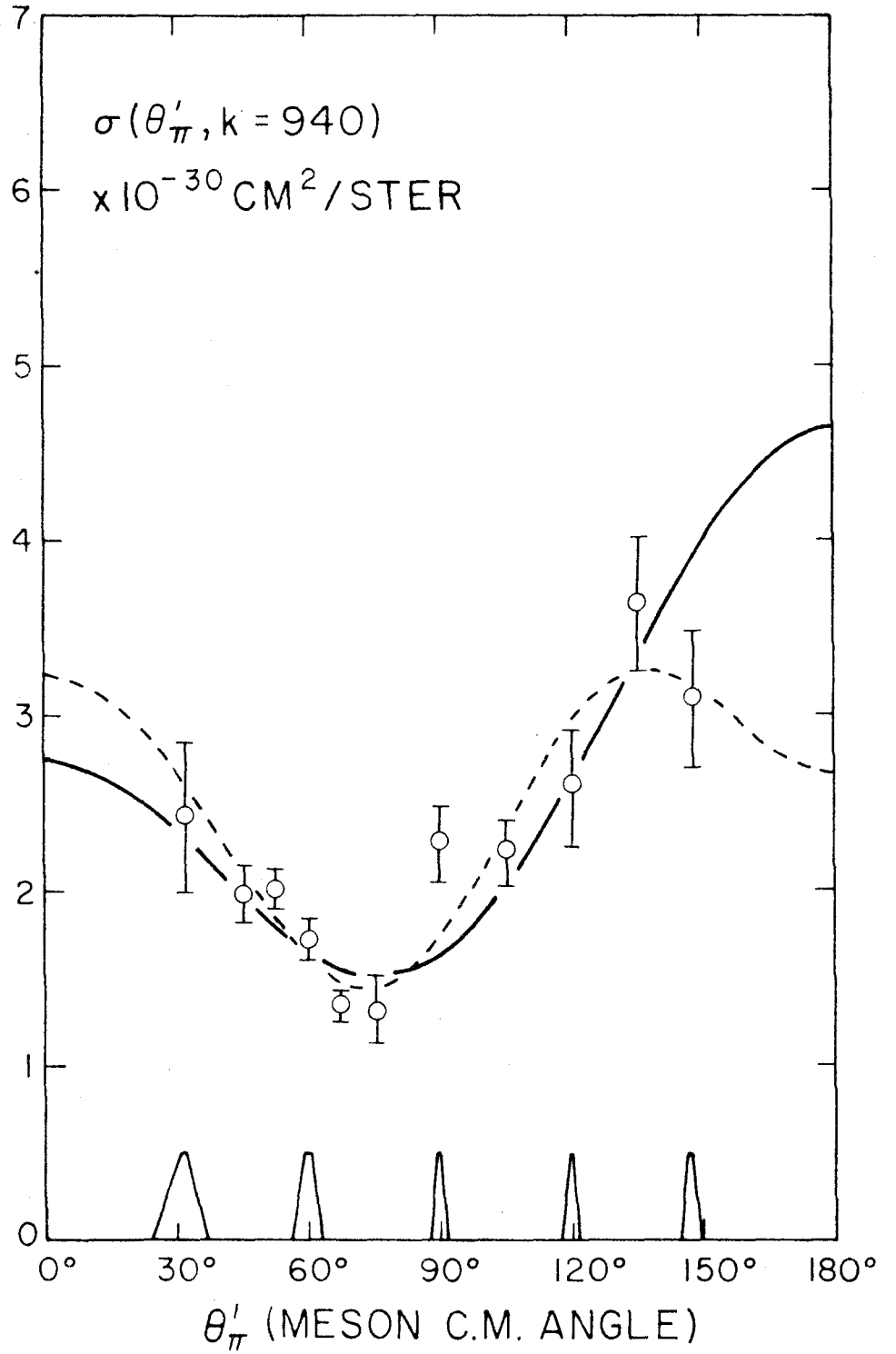
$\sigma(\theta'_\pi, k = 940)$
$\times 10^{-30}$ CM^2/STER
7
6
5
4
3
2
1
0
0°
30°
60°
90°
120°
150°
180°
θ'_π (MESON C.M. ANGLE)

Figure 21. Kinematics for the Reaction $\gamma + P \longrightarrow \pi^o + P$

The solid curves give the proton laboratory momentum versus laboratory angle at constant photon laboratory energies. The dotted curves gives the same relation at constant pion C.M. angles.

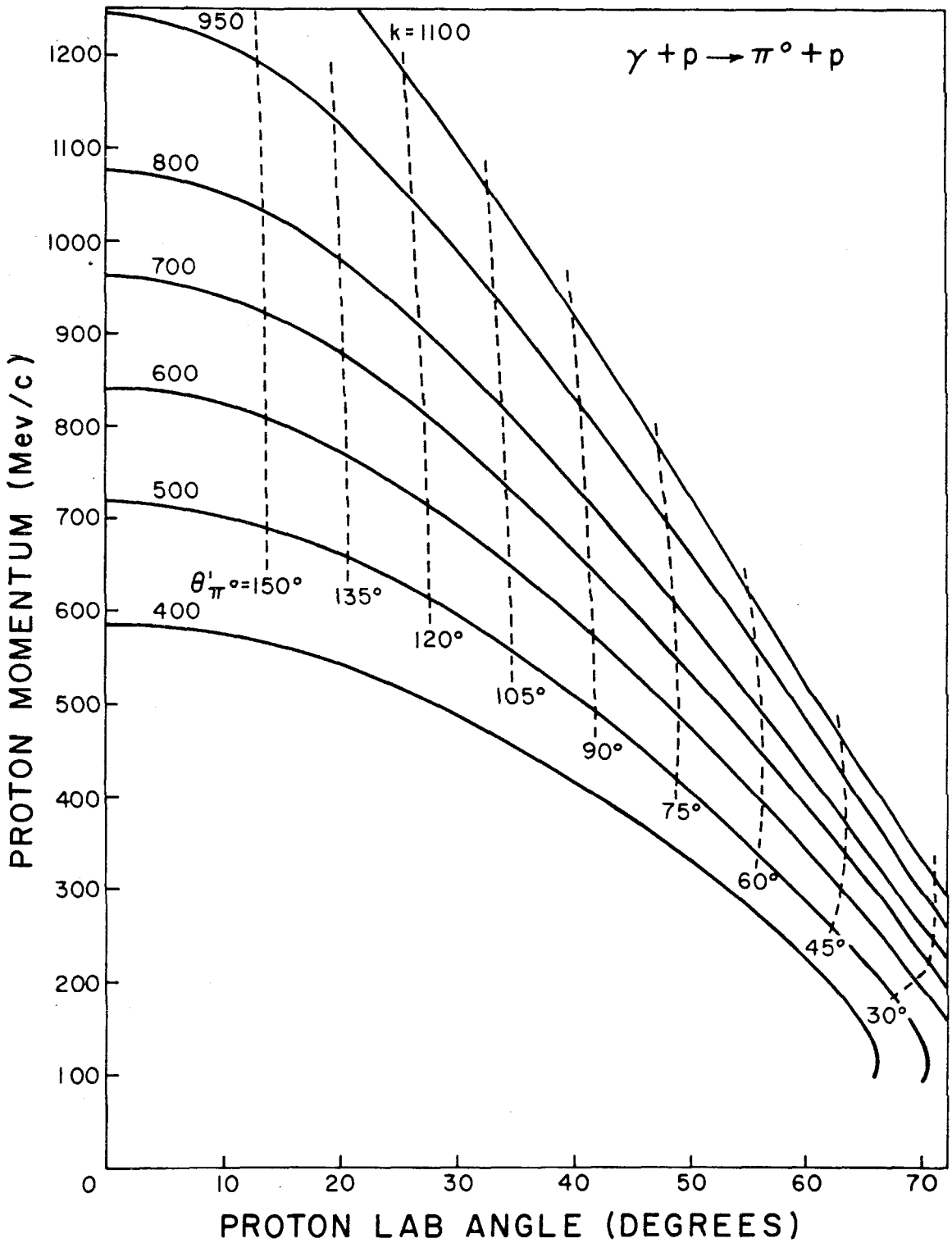
950
k=1100
800
700
600
500
400
θ'_{π^0}=150°
135°
120°
105°
90°
75°
60°
45°
30°
$\gamma + p \rightarrow \pi^0 + p$
PROTON MOMENTUM (Mev/c)
PROTON LAB ANGLE (DEGREES)
0
100
200
300
400
500
600
700
800
900
1000
1100
1200
10
20
30
40
50
60
70

TABLE III.

This table lists the values of the cross section used in the angular distributions. The central k values are given in Mev. Most of the points are direct measurements but a few are interpolations of the excitation functions. The errors are the combined B and C type errors defined on page 58.

Table III.

C.M. Differential Cross Sections Used in Angular Distributions (in Units $10^{-30}cm^2$/Ster.)

θ'_π	k = 490	585	690	785	940
31.5°	-	-	2.10 ± .60	2.45 ± .60	2.42 ± .43
37°	-	-	2.30 ± .50	2.67 ± .60	-
45°	4.55 ± .46	2.68 ± .40	1.75 ± .25	1.96 ± .17	1.98 ± .16
52.5°	-	2.10 ± .29	2.50 ± .30	2.61 ± .16	2.01 ± .11
60°	3.94 ± .36	2.54 ± .25	2.55 ± .25	2.53 ± .15	1.72 ± .12
67.5°	5.00 ± .28	2.75 ± .24	2.27 ± .38	2.41 ± .13	1.36 ± .08
75°	5.06 ± .35	2.56 ± .22	2.85 ± .28	3.11 ± .15	1.32 ± .19
90°	5.43 ± .41	3.27 ± .26	3.88 ± .41	4.07 ± .21	2.27 ± .21
105°	-	-	3.39 ± .30	3.62 ± .24	2.22 ± .19
113°	-	-	-	3.32 ± .30	-
120°	4.65 ± 1.07	2.90 ± .57	2.90 ± .36	3.12 ± .34	2.59 ± .33
135°	-	-	2.77 ± .41	2.34 ± .41	3.64 ± .38
147°	1.92 ± 1.73	.32 ± .56	2.00 ± .47	1.94 ± .45	3.09 ± .40

two lower energies to get a good angular distribution.

It is certainly reasonable to expect partial waves with $\ell > 1$ to be important at the energies under investigation (see following section). Consequently the angular distributions were fit to an expression of the form

$$\sigma(k, \theta_\pi') = \sum_{n=0}^{m} A_n(k) \cos^n \theta_\pi' \qquad (2)$$

by the principle of maximum likelihood (frequently called least squares). The maximum value of m that was tried was m = 4 for k = 490 and 585 Mev. and m = 6 for the other values of k. This was done on the Electrodata computer with a program coded by W. Wales.

In an attempt to decide what value of m gives the most reasonable fit to the data a number of factors were considered. Some of the fits give a negative cross section outside of the measured regions. No attempt was made to refit the data with the constraint that the cross section not be negative for those values of m. The chi-squared goodness of fit test (27) was applied to the fits and the results are summarized in Table IV. There are not enough data at the two lower energies for this test to be very good. However a value of m = 2 is certainly consistent with the data on the basis of this test. The m = 4 fit for the 490 Mev. data has a very strong forward peak mainly due to the 60° point, which seems very low. The m = 3 fit goes negative at 165° while the m = 3 and 4 fits for the 585 Mev. data go negative around 150°. On the basis of χ_e^2 the fit of the 690 Mev. data is not improved

TABLE IV.

This table summarizes the chi-squared goodness of fit test. The photon energy in Mev. is listed in the first column. The second column gives the highest power of $\cos\theta'_\pi$ used in the fit; an asterisk indicates that particular fit gives a negative cross section outside the region of measurement. The third column gives the quantity

$$\chi^2_e = \sum_{i=1}^{s} \left[\frac{\sigma(\theta'_i) - \sigma_f(\theta'_i)}{\epsilon_i} \right]^2$$

where $\sigma(\theta'_\pi)$ is the measured cross section and $\sigma_f(\theta'_\pi)$ is the value calculated by the fit at $\theta'_\pi = \theta'_i$. The quantity s is the number of measured points in the angular distribution and ϵ_i is the combined B and C type errors for the measurement at each angle. The next column gives the expected value for χ^2_e and the last column lists the probability that χ^2_e could have a larger value than that listed in the third column if it has a chi-squared distribution. A small value of this quantity means the fit is very unlikely. The quantities in the parentheses are the results of the goodness of fit test with several suspicious points suppressed. See the text for a discussion of these points.

Table IV.

Chi-Squared Goodness of Fit Test

k	m	χ_e^2	$\chi_{.5}^2$	$P(\chi^2 > \chi_e^2)$
490	2	6.5	3.4	0.18
490	3*	3.4	2.4	0.34
490	4	3.3	1.4	0.20
585	2	9.1	4.4	0.11
585	3*	3.2	3.4	0.53
585	4*	2.8	2.4	0.36
690	2	9.2	8.3	0.42
690	3	8.1	7.3	0.42
690	4	6.6	6.3	0.47
690	5	6.6	5.3	0.36
690	6	6.6	4.4	0.26
785	2	35.7(19.3)	9.3(7.3)	$<$0.01(.01)
785	3*	26.8(12.6)	8.3(6.3)	$<$0.01(.08)
785	4	17.9(6.5)	7.3(5.3)	0.02(.37)
785	5	15.5(7.5)	6.3(4.4)	0.03(.19)
785	6	13.8(7.5)	5.3(3.4)	0.04(.11)
940	2	26.1(16.9	7.3(6.3)	$<$0.01(.02)
940	3	17.2(11.8)	6.3(5.3)	0.02(.07)
940	4	16.1(9.3)	5.3(4.4)	0.01(.11)
940	5	14.3(9.3)	4.4(3.4)	0.01(.05)
940	6*	10.5(8.8)	3.4(2.4)	0.03(.03)

by taking values of m larger than 4.

It was surprising to see that the higher energy data have such large values for χ^2_e. The two 785 Mev. points at 52.5° and 67.5° give a very large contribution to χ^2_e; if the χ^2_e contribution of these two points is suppressed then the test (shown in parentheses in Table VI) indicates that m = 4 gives a good fit and larger values of m do not improve the fit. If the data were fit without these two points, χ^2_e would be even smaller than that indicated in the parentheses. The 52.5°, 60° and 67.5° points were run very close together. Individual runs at each point were very consistent and the backgrounds were very small. The one point that gives a large contribution to χ^2_e for the 940 Mev. data is the 90° point. The individual runs at this point also showed fairly good consistency. The χ^2 test without this point is also given in Table VI. Here again values of m larger than 4 do not improve the fit.

Although the evidence is by no means conclusive, it seems that m values no larger than 4 are necessary to fit the data. The fits for m = 2 and 4 are shown in figures 16 - 20 with one exception. The m = 4 fit for 490 Mev. reaches a value of $7 \times 10^{-30} cm^2/ster.$ at 0°; for convenience of plotting the m = 3 curve is shown instead. McDonald (28) obtained a good fit to the 450 Mev. OM data with m = 2 that showed a slight tendency toward a rise in the forward θ'_π direction.

To further examine the fits to the angular distributions, the coefficients $A_n(k)$ for the curves drawn in figures 16 - 20 are plotted in figures 22 and 23 along with the values obtained by McDonald for

Figures 22-23. Angular Distribution Coefficients

The coefficients $A_n(k)$ obtained by fitting the data with the formula

$$\sigma(\theta'_\pi, k) = \sum_{n=o}^{m} A_n(k) \cos^n \theta'_\pi$$

are plotted versus photon energy. The open circles are the values obtained from the OM data by McDonald (28). The solid circles are the values obtained in this experiment using an $m = 3$ fit at 490 Mev. and $m = 4$ fit for all the other energies investigated. The triangles are the values obtained by using an $m = 2$ fit for all the data. The solid curves are best eye fits assuming $m = 2$ fits below 600 Mev. and $m = 4$ fits above this energy.

Figure 22. A_o and A_2 Versus k

Where no errors are shown, they are smaller than the points.

Figure 23. A_1, A_3 and A_4 Versus k

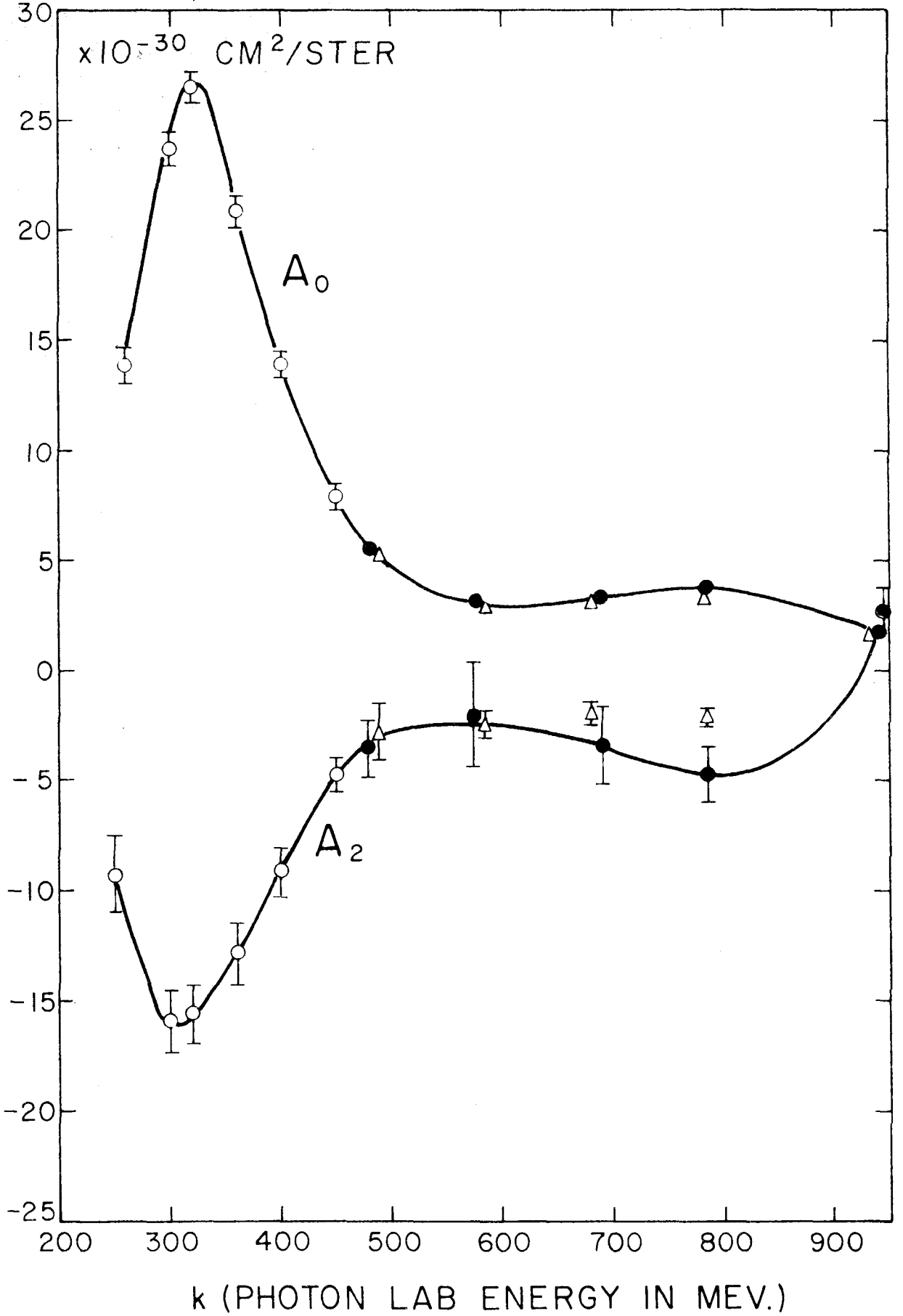
x10⁻³⁰ CM²/STER
30
25
20
15
10
5
0
-5
-10
-15
-20
-25
A₀
A₂
200
300
400
500
600
700
800
900
k (PHOTON LAB ENERGY IN MEV.)

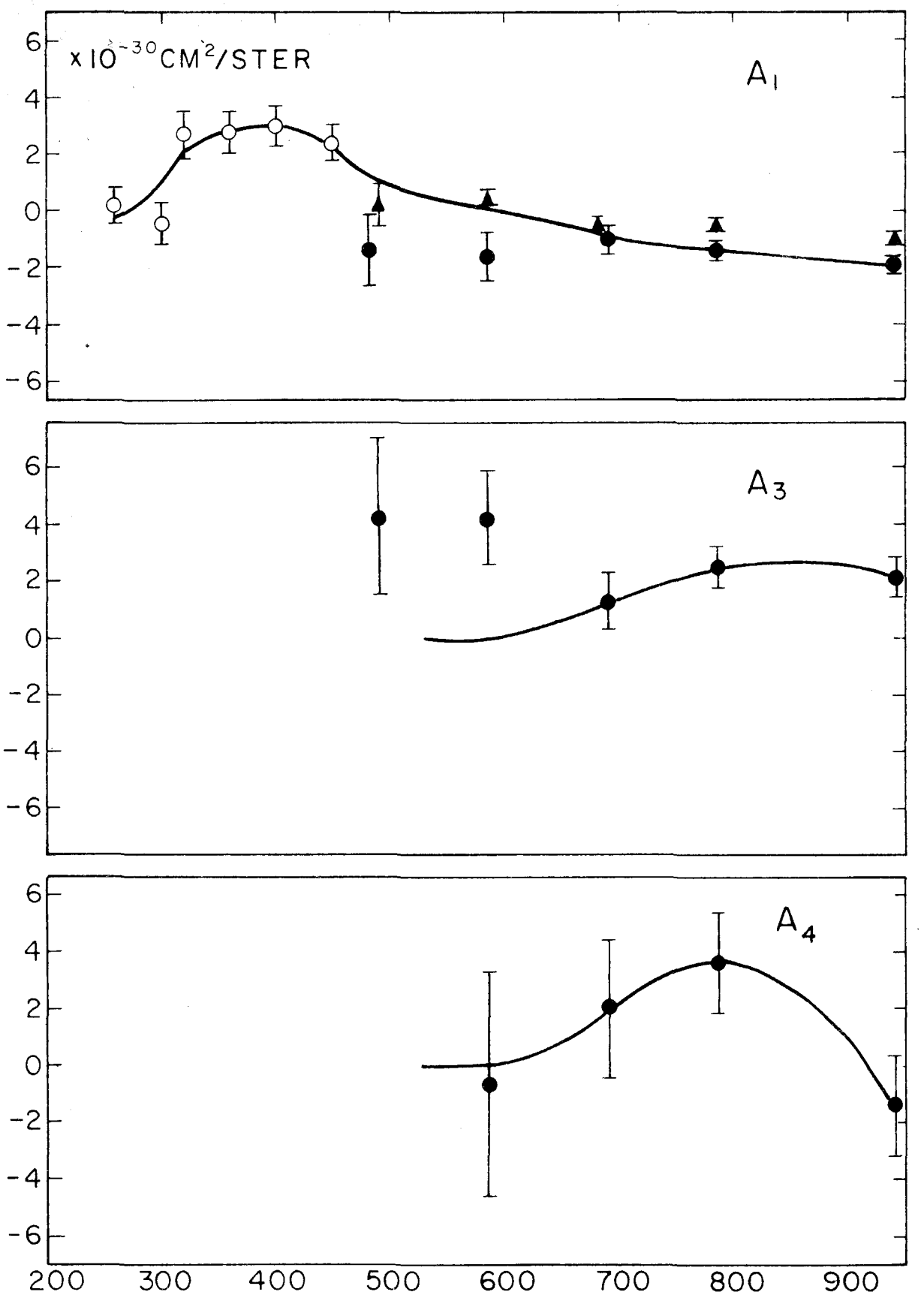
x 10^-30 CM^2/STER
A1
A3
A4
6
4
2
0
-2
-4
-6
200
300
400
500
600
700
800
900
k (PHOTON LAB ENERGY IN MEV.)

the OM data. If one assumes that only m = 2 is necessary for energies below 600 Mev. and m = 4 for higher energies, both A_3 and A_4 have reasonable shapes. It is believed that this is the best interpretation of the angular distributions.

Once the fit to the angular distribution has been obtained, the total cross section can be calculated from the formula

$$\sigma_T = 4\pi (A_o + \frac{1}{3} A_2 + \frac{1}{5} A_4) \qquad (3)$$

The values of the coefficients selected and the total cross sections obtained by substituting these values in equation 3 are given in Table V. The total cross sections obtained by all the fits including the m = 6 fits are all within the statistical error of the values given in Table V. The total cross section is plotted in figure 24 along with that obtained from the OM data.

It is apparent that the 'resonance tail' is contributing to the total cross section above 600 Mev. In order to see if the rise above 600 Mev. is a broad peak riding on top of the 'resonance tail', it is necessary to subtract out the effects of the (3, 3) resonance. This has been done by using the one level dispersion formula given by Gell-Mann and Watson (29). It is realized that the justification of this type of formula is difficult to establish in a relativistic region and it has been used only to provide a definite way of making the subtraction. The solid curve of figure 24 has been obtained from the formula

$$= 2\pi \lambda^2 \frac{\Gamma \Gamma_\gamma}{(T - T_o)^2 + \Gamma^2/4} \qquad (4)$$

TABLE V.

This table gives the angular distribution coefficients obtained for the data by assuming only terms up to $\cos^2\theta'_\pi$ are necessary below k = 600 Mev. and terms up to $\cos^4\theta'_\pi$ are necessary above this energy. The total cross sections obtained from an integration of these angular distributions are given in the last column.

Table V.

Angular Distribution Coefficients and Total Cross Sections
(Units of 10^{-30} cm^2/Ster.)

k	A_0	A_1	A_2	A_3	A_4	$\sigma_T \times 10^{30}$
490	5.20 ± .27	0.23 ± .71	-2.7 ± 1.3			53.8 ± 5.1 cm^2
585	2.95 ± .18	0.41 ± .31	-2.4 ± 0.6			26.9 ± 2.1
690	3.43 ± .23	-1.00 ± .51	-3.3 ± 1.7	1.3 ± 1.0	2.0 ± 2.4	34.2 ± 1.8
785	3.70 ± .14	-1.36 ± .34	-4.7 ± 1.2	2.5 ± 0.7	3.6 ± 1.8	36.1 ± 1.5
940	1.72 ± .13	-1.88 ± .33	2.7 ± 1.1	2.2 ± 0.7	-1.4 ± 1.7	29.1 ± 1.3

Figure 24. Total Cross Section for the Reaction $\gamma + P \longrightarrow \pi^o + P$

The total cross sections obtained by integrating the angular distributions are plotted versus k. The open circles are those given by McDonald for the OM data. The solid circles are the results of this experiment. The solid curve is calculated from a one level dispersion formula of the type given by Watson and Gell-Mann (29). The dotted curve is the difference between the total cross section and the solid curve and is taken to represent the contribution not due to the (3, 3) resonance.

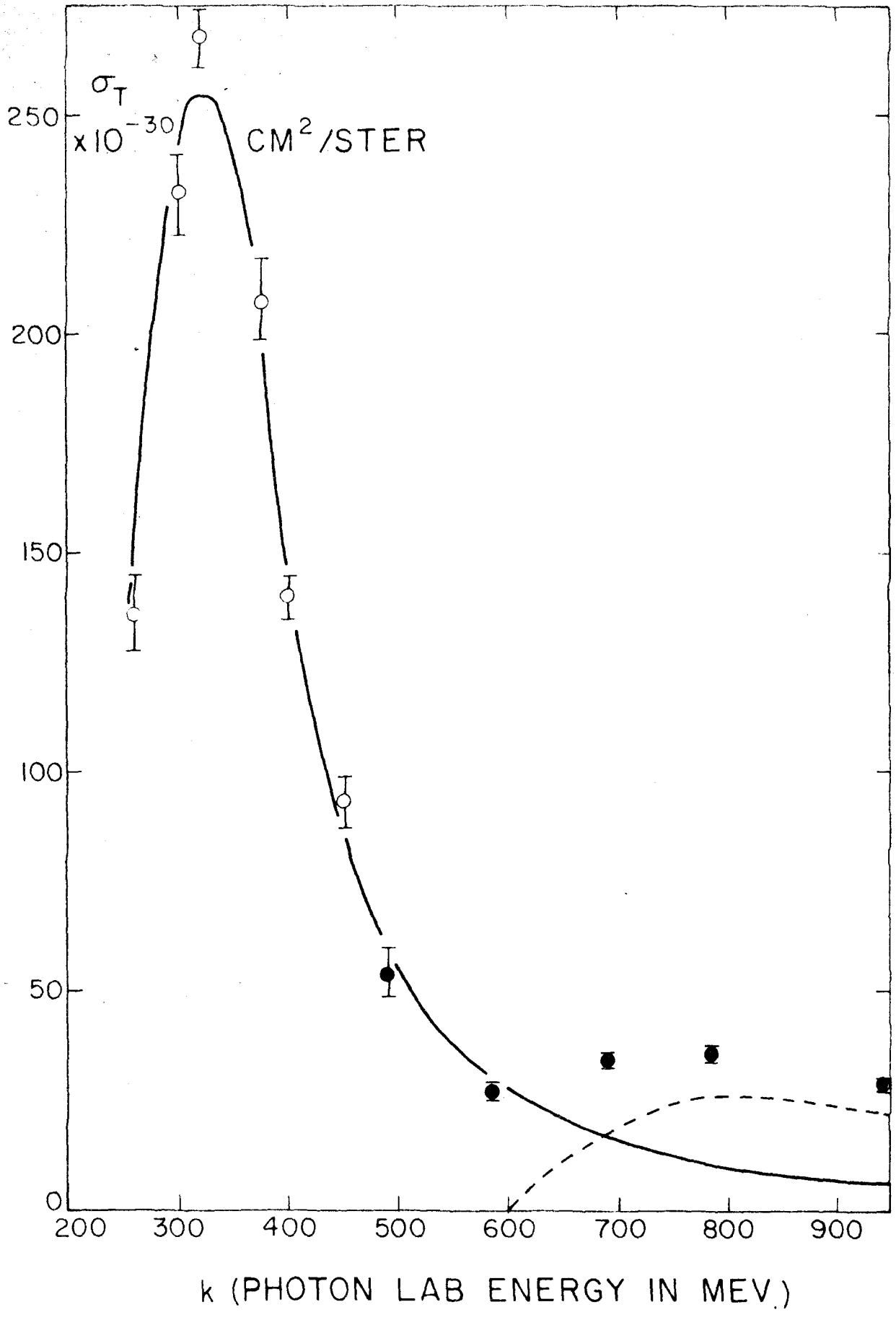
σ_T
$\times 10^{-30}$ CM^2/STER
250
200
150
100
50
0
200
300
400
500
600
700
800
900
k (PHOTON LAB ENERGY IN MEV.)

where $2\pi\lambda\!\!\!^{-}$ is the C.M. photon wave length, T is the sum of the C.M. photon energy and the nucleon C.M. kinetic energy,

$$\Gamma = \frac{2(a/\lambda\!\!\!^{-})^3}{1 + (a/\lambda\!\!\!^{-})^2} \, b \tag{5}$$

and

$$\Gamma_\gamma = \frac{\left[\hbar / mc\right]^2}{1 + (a/\lambda\!\!\!^{-})^2} \, c' \tag{6}$$

T_o, a, b and c′ are parameters whose values in this calculation are $(170 + mc^2)$ Mev., .88 h/mc, 150 Mev. and .27 Mev., respectively. The dotted curve in figure 24 is obtained by subtracting the solid curve from the total cross section. It is seen that a broad peak starting at 600 Mev. accounts for the rise in the total cross section above this energy.

Before discussing the possible significance at this point or attempting to interpret the angular distributions, some theoretical relationships will be described in the next section.

IX. THEORY

In order to see what theoretical relationships might be valid for photoproduction at high energies, it will be useful to discuss the basis of our understanding of these processes below 450 Mev. Much of this understanding has been achieved through the development of general relationships between photoproduction and meson-nucleon scattering. The scattering of the different types of pions is most easily discussed in terms of the isotopic spin formalism which was first applied to mesons by Kemmer (30). A system comprised of one pion and one nucleon can have six possible charge configurations which are given in Table VI in terms of pure isotopic spin states.

Table VI.

	I = 3/2	I = 1/2
$I_z = +3/2$	$P\pi^+$	
$I_z = +1/2$	$\sqrt{2/3}P\pi^o - \sqrt{1/3}N\pi^+$	$\sqrt{1/3}P\pi^o + \sqrt{2/3}N\pi^+$
$I_z = -1/2$	$\sqrt{1/3}P\pi^- + \sqrt{2/3}N\pi^o$	$\sqrt{2/3}P\pi^- - \sqrt{1/3}N\pi^o$
$I_z = -3/2$	$N\pi^-$	

Here N and P refer to the two charge states of the nucleon and $\pi^{\pm, o}$ refer to the three meson charge states. The hypothesis of charge independence means that I, the total isotopic spin, is a good quantum number for the meson-nucleon interaction and that the scattering amplitudes depend on I but are independent of I_z. This principle

reduces to two the number of independent scattering amplitudes for a given orbital (ℓ) and total (j) angular momentum. For laboratory pion energies below 300 Mev. only S and P waves are important (31), and the data can be characterized by the two S wave phase shifts, δ_1 and δ_3, and the four P wave phase shifts, δ_{11}, δ_{13}, δ_{31} and δ_{33}. The subscript for an S wave phase shift refers to twice the value of the isotopic spin as does the first subscript of a P wave phase shift; the second subscript refers to twice the value of the total angular momentum.

Although meson photoproduction occurs by the absorption of a photon, the meson-nucleon interaction is involved in a very direct way. Even though the total isotopic spin is not conserved in electromagnetic interactions (I_z is conserved), Watson (32) applied the isotopic spin formalism to meson photoproduction and showed that the four basic reactions:

I. $\gamma + P \longrightarrow \pi^+ + N$

II. $\gamma + N \longrightarrow \pi^- + P$

III. $\gamma + P \longrightarrow \pi^o + P$

IV. $\gamma + N \longrightarrow \pi^o + N$

are related by three independent amplitudes if charge independence is valid. The Roman numerals will be used to denote the reactions. The amplitudes, T, are given by:

$$T(I) = \sqrt{2}t(3) + 1/\sqrt{2}t(1) - \sqrt{2}\delta t(1) \qquad (1)$$

$$T(II) = \sqrt{2}t(3) + 1/\sqrt{2}t(1) + \sqrt{2}\delta t(1) \qquad (2)$$

$$T(III) = 2t(3) - 1/2t(1) + \delta t(1) \qquad (3)$$

$$T(IV) = 2t(3) - 1/2t(1) - \delta t(1) \qquad (4)$$

where $\delta t(1)$ is an amplitude which arises from nucleon recoil and leads to final states of isotopic spin $I = 1/2$; $t(1)$ and $t(3)$ are amplitudes which give rise to final states of $I = 1/2$ and $I = 3/2$, respectively. Equations 1 - 4 can be written in a more concise form by the use of 2 x 2 matrices in nucleon isotopic spin space. For example Chew, Goldberger, Low and Nambu (33) write a general single meson photoproduction amplitude as

$$A = A^{+}\not{\tau}^{+} + A^{-}\not{\tau}^{-} + A^{o}\not{\tau}^{o} \qquad (5)$$

where $\not{\tau}^{\pm, o}$ are the isotopic spin matrices whose elements are given in Table VII. The $A^{\pm, o}$ are just three linearly independent combinations of $t(3)$, $t(1)$ and $\delta t(1)$.

Table VII.

Reaction	I	II	III	IV
Matrix				
$\not{\tau}^{+}$	1	1	0	0
$\not{\tau}^{-}$	0	0	$\sqrt{2}$	$-\sqrt{2}$
$\not{\tau}^{o}$	1	-1	$\sqrt{2}$	$\sqrt{2}$

The experimental results of photomeson production have been analyzed by phenomenological theories and specific meson theories. Both of these approaches show that photoproduction is related to

meson-nucleon scattering through the phase shifts. Using the facts that the pion is pseudoscalar (34, 35) and has zero spin (36), Feld (37) has made an analysis on the basis of angular momentum considerations. The results are summarized in Table VIII where the total angular momentum and parity of the intermediate state are given in the second column and the angular distribution, $W(\theta'_\pi)$, is given in the fourth column. The first subscript on the amplitude gives the order of the multipole and the second subscript gives twice the total angular momentum. The isotopic spin index, when shown, will be the value 2I enclosed in parentheses. When a mixture of states occurs, the angular distribution is complicated by interference terms.

Table VIII.

γ-Ray Absorbed	Intermediate State	ℓ of meson	$W(\theta'_\pi)$	Amplitude
Mag. dipole	1/2 +	1	constant	M_{11}
Mag. dipole	3/2 +	1	$5- 3\cos^2\theta'_\pi$	M_{13}
Elect. dipole	1/2 -	0	constant	E_{11}
Elect. dipole	3/2 -	2	$5- 3\cos^2\theta'_\pi$	E_{13}
Elect. quad.	3/2 +	1	$1+ \cos^2\theta'_\pi$	E_{23}
Elect. quad.	5/2 +	3	$1+ 6\cos^2\theta'_\pi - 5\cos^4\theta'_\pi$	E_{25}

If meson production occurs only in S and P states, Gell-Mann and Watson (29) have shown that the angular distribution is given by

$$W(\theta') = |E_{11}|^2 + |M_{11}|^2 + 1/2|M_{13}|^2 (5 - 3\cos^2\theta'_\pi)$$

$$1/8|E_{23}|^2 (1 + \cos^2\theta'_\pi)$$

$$- 2\mathrm{Re}\, E^*_{11} (M_{13} - M_{11} - 1/2E_{23}) \cos\theta'_\pi$$

$$- 1/2\mathrm{Re}\, E^*_{23} (M_{13} - M_{11}) (3\cos^2\theta'_\pi - 1)$$

$$- \mathrm{Re}\, M^*_{13}M_{11} (3\cos^2\theta'_\pi - 1) \qquad (6)$$

Watson (38) has shown that the phase of each multipole amplitude is given by the scattering phase shift of the corresponding final state. For example $M_{13}(3)$ is the magnetic dipole amplitude which produces a meson-nucleon state with $j = 3/2$, $\ell = 1$, $I = 3/2$ and it can be written as

$$M_{13}(3) = |M_{13}(3)| e^{i\delta_{33}} \qquad (7)$$

Watson, Keck, Tollestrup and Walker (39) have analyzed the photomeson data below 400 Mev. from hydrogen and deuterium with a model that considers the pion-nucleon state with $\ell = 1$, $j = 3/2$, $I = 3/2$ to be one of strong, attractive interaction. This state is generally referred to as the (3, 3) state. By expanding the cross sections in terms of the multipole amplitudes and phase shifts and using the measured values for the phase shifts, they were able to find the various multipoles from the data. The results, which were obtained before the data of McDonald, Peterson and Corson were available,

indicated that both $M_{13}(3)$ and $E_{23}(3)$ were important.

Chew and Low (40, 41) developed a cutoff Yukawa type meson theory of pseudoscalar mesons with pseudovector coupling. The theory achieves some simplicity by eliminating nucleon-antinucleon pairs and nucleon recoil. Instead of the many (multipole) parameters of the phenomenological theory of Watson et al, their theory contains only two, the renormalized coupling constant and the pion cutoff momentum. In this static theory the dependence of the photomeson cross sections on the scattering phase shifts is explicit. This theory has had some success (42) in correlating meson scattering and photoproduction. Recently Chew, Goldberger, Low and Nambu (33) have applied the dispersion relations to both scattering and photoproduction. By assuming that the (3, 3) resonance not only dominates but exhausts the dispersion integrals, they have been able to obtain the equations which in the limit of infinite nucleon mass are those derived by the static theory. One advantage of this new method is that the nucleon recoil effects can be included in an unambigious way. McDonald (28) has used this theory and the measured phase shifts to calculate the angular distribution for π^o production up to 450 Mev. and has found that the agreement with the OM data is very good. Since the electric quadrupole term has not been explicitly calculated by this theory, it has not been included in McDonald's work.

Unfortunately the successful techniques just discussed fail in higher energy regions. The (3, 3) resonance is falling off rapidly and cannot be expected to dominate as it does around 300 Mev. Scattering

phase shifts become complex when an additional meson can be formed in the scattering process further complicating the picture. Experiments on π^- - P scattering at 1.0 Bev. pion lab kinetic energy show that ratio of scattering with production of an additional meson to scattering which results in only one meson in the final state is about 0.6 (43). Consequently phase shifts are known to be complex in this region.

However one can proceed to develop formulas similar to equation 6 which include higher partial waves. This will prove to be useful in the event that at most one or two multipole amplitudes are non-zero in this higher energy region; if this is the case it will be possible to identify them by means of the angular distributions. Moravcsik (44) has pointed out that a partial wave analysis for charged photomeson production is complicated by a retardation term which arises from the interaction of the photon with the meson current. Since no such term appears in neutral production, a normal partial wave analysis can be made.

Because the range of the interaction between mesons and nucleons is not expected to be much greater than the meson Compton wavelength, angular momentum greater than

$$\ell = \frac{\hbar/mc}{\lambda} \tag{8}$$

(where $2\pi\lambda$ is the meson deBroglie wavelength) are not expected to be important. The above expression gives $\ell = 2, 3, 4$ at photon lab energies of 390, 650, 960 Mev., respectively. It was seen in the last section that the data could be fit by considering $\ell \leq 2$. Consequently,

a multipole expansion including only S, P and D waves will suffice.

A very general expression for the photoproduction amplitude of a single meson can be written down without recourse to a specific meson theory. The general arguments are given in detail by Chew et al (33) and will be briefly summarized here. In this section all the quantities will be written in the C. M. system.

The most general S-matrix elements must be comprised of Lorentz invariant quantities. The available four-vector variables in the photoproduction of a spin zero meson are:

1. Incident photon momentum, k
2. Photon polarization, ϵ
3. Initial nucleon momentum, p_1
4. Final nucleon momentum, p_2
5. Outgoing pion momentum, q
6. Nucleon Dirac operator, γ

The possible number of independent scalars which can be formed from these variables is restricted by the Dirac equation, momentum-energy conservation and the equations:

$$p_1^2 = p_2^2 = - M^2 \tag{9}$$

$$q^2 = - m^2 \tag{10}$$

$$k^2 = 0 \tag{11}$$

where m and M are the meson and nucleon mass, respectively. Using the fact that the matrix element must be linear and homogeneous in ϵ

and invoking the requirement of gauge invariance, Chew et al write down the four allowed forms as:

$$M(1) = i\gamma_5 \gamma \cdot \epsilon \ \gamma \cdot k \tag{12}$$

$$M(2) = 2i\gamma_5 (P \cdot \epsilon \ q \cdot k - P \cdot k \ q \cdot \epsilon) \tag{13}$$

$$M(3) = \gamma_5 (\gamma \cdot \epsilon \ q \cdot k - \gamma \cdot k \ q \cdot \epsilon) \tag{14}$$

$$M(4) = 2\gamma_5 (\gamma \cdot \epsilon \ P \cdot k - \gamma \cdot k \ P \cdot \epsilon - iM\gamma \cdot \epsilon \ \gamma \cdot k) \tag{15}$$

where

$$P = 1/2(p_1 + p_2) \tag{16}$$

and the γ_5 appears because the mesons are pseudoscalar.

The complete invariant photomeson transition matrix element is written as

$$\langle u_2 | H | u_1 \rangle = \sum_{i=1}^{4} \langle u_2 | M(i) | u_1 \rangle \ A(i) \tag{17}$$

where u_1 and u_2 are the initial and final nucleon spinors, respectively. The A(i)'s are functions of $P \cdot k$, $q \cdot k$ and the nucleon isotopic spin. The isotopic spin can be made explicit by writing each A in the form given by equation 5. The differential cross section is written as

$$\frac{d\sigma}{d\Omega'} = \left| \langle 2 | F | 1 \rangle \right|^2 \tag{18}$$

where F can be expressed

$$F = i \bar{\sigma} \cdot \bar{\epsilon} \, F_1 + \frac{\bar{\sigma} \cdot \bar{q} \ \bar{\sigma} \cdot (\bar{k} \times \bar{\epsilon}) F_2}{qk} + \frac{i \bar{\sigma} \cdot \bar{k} \ \bar{q} \cdot \bar{\epsilon} \ F_3}{qk} + \frac{i \bar{\sigma} \cdot \bar{q} \ \bar{q} \cdot \bar{\epsilon} \ F_4}{q^2} \tag{19}$$

Here the vector quantities are the regular three-vector equivalents of the terms defined earlier and σ is the Pauli spin matrix. The quantities F_1, F_2, F_3, F_4 are given in terms of the derivatives of the Legendre polynomials by the formulas:

$$F_1 = \sum_{\ell=0}^{\infty} (\ell M_{\ell+} + E_{\ell+}) P'_{\ell+1}(x) + \left[(\ell+1) M_{\ell-} + E_{\ell-}\right] P'_{\ell-1}(x) \tag{20}$$

$$F_2 = \sum_{\ell=0}^{\infty} \left[(\ell+1) M_{\ell+} + \ell M_{\ell-}\right] P'_{\ell}(x) \tag{21}$$

$$F_3 = \sum_{\ell=0}^{\infty} (E_{\ell+} - M_{\ell+}) P''_{\ell+1}(x) + (E_{\ell-} + M_{\ell-}) P''_{\ell-1}(x) \tag{22}$$

$$F_4 = \sum_{\ell=0}^{\infty} (M_{\ell+} - E_{\ell+} - M_{\ell-} - E_{\ell-}) P''_{\ell}(x) \tag{23}$$

where x is the cosine of the angle that the pion makes with the direction defined by the incident photon. The energy dependent amplitudes $M_{\pm}$ and $E_{\pm}$ refer to the transitions caused by the absorption of magnetic and electric radiation leading to states of orbital angular momentum ℓ and total angular momentum $\ell \pm 1/2$. Each of the $M^{\pm}$'s and $E^{\pm}$'s can be written in the isotopic spin notation by means of equation IX-5. After evaluating equations 20 - 23 for $\ell \leq 2$ and substituting in equation 19, an average over initial spins and polarizations and a sum over final spins yields

$$\frac{d\sigma}{d\Omega'} = A_o + A_1\cos\theta_\pi' + A_2\cos^2\theta_\pi' + A_3\cos^3\theta_\pi' + A_4\cos^4\theta_\pi' \tag{24}$$

where θ_π' is the pion C.M. angle and:

$$A_o = \left|E_{o+}\right|^2 + 9/2\left|E_{1+}\right|^2 + \left|M_{1-}\right|^2 + 5/2\left|M_{1+}\right|^2 + 5/2\left|E_{2-}\right|^2 + 45/4\left|E_{2+}\right|^2$$
$$+ 9/2\left|M_{2-}\right|^2 + 9/2\left|M_{2+}\right|^2 + 3\mathrm{Re}\, E_o^* (M_{2-} - M_{2+} - \frac{E_{2-}}{3} - 2E_{2+})$$
$$- 3\mathrm{Re}\, E_{1+}^* (M_{1+} - M_{1-}) + 3/2\,\mathrm{Re}\, E_{2+}^* (3M_{2+} - 3M_{2-} + 5E_{2-})$$
$$+ 3\mathrm{Re}\, E_{2-}^* (M_{2-} - M_{2+}) + \mathrm{Re}\, M_{1+}^* M_{1-} - 9\mathrm{Re}\, M_{2+}^* M_{2-} \tag{25}$$

$$A_1 = 2\mathrm{Re}\, E_{o+}^* (M_{1+} - M_{1-} + 3E_{1+})$$
$$+ 6\mathrm{Re}\, E_{1+}^* (3E_{2+} + 3M_{2-} - 3M_2 - 2E_{2-})$$
$$+ 2\mathrm{Re}\, E_{2-}^* (M_{1+} - M_{1-}) + 18\mathrm{Re}\, E_{2+}^* (M_{1-} - M_{1+})$$
$$+ 6\mathrm{Re}\, M_{1+}^* (3M_{2+} + 2M_{2-}) + 9\mathrm{Re}\, M_{1-}^* (M_{2+} + 2M_{2-}) \tag{26}$$

$$A_2 = 9/2\left|E_{1+}\right|^2 - 3/2\left|M_{1+}\right|^2 - 3/2\left|E_{2-}\right|^2 + 27/2\left|E_{2+}\right|^2 + 27\left|M_{2+}\right|^2$$

$$+ 9/2\left|M_{2-}\right|^2 + 3\mathrm{Re}\, E^*_{o+}\,(6E_{2+} + E_{2-} + 3M_{2+} - 3M_{2-})$$

$$+ 9\mathrm{Re}\, E^*_{1+}\,(M_{1+} - M_{1-}) - 3\mathrm{Re}\, M^*_{1+}\, M_{1-}$$

$$- 9\mathrm{Re}\, E^*_{2+}\,(9M_{2+} - 9M_{2-} + 7E_{2-}) + 9\mathrm{Re}\, E^*_{2-}\,(M_{2+} - M_{2-})$$

$$+ 81\mathrm{Re}\, M^*_{2+}\, M_{2-} \qquad (27)$$

$$A_3 = 18\mathrm{Re}\, E^*_{1+}\,(E_{2+} + 2M_{2+} - 2M_{2-} + E_{2-})$$

$$+ 30\mathrm{Re}\, E^*_{2+}\,(M_{1+} - M_{1-}) - 6\,\mathrm{Re}\, M^*_{1+}\,(2M_{2+} + 3M_{2-})$$

$$- 15\mathrm{Re}\, M^*_{1-}\, M_{2+} \qquad (28)$$

$$A_4 = 45/4\left|E_{2+}\right|^2 - 45/2\left|M_{2+}\right|^2 + 225/2\,\mathrm{Re}\, E^*_{2+}\,(M_{2+} - M_{2-} + E_{2-})$$

$$- 90\,\mathrm{Re}\, M^*_{2+}\, M_{2-} \qquad (29)$$

These results can be compared with those of Gell-Mann and Watson given in equation 6 by making the substitutions:

$$E_{o+} = E_{11}$$

$$3E_{1+} = 1/2\, E_{23}$$

$$M_{1-} = - M_{11}$$

$$M_{1+} = - M_{13}$$

and equating all the other terms to zero. The results are consistent with the fact that the highest power of $\cos \theta'_{\pi}$ that can appear in the angular distribution is $2j - 1$ when j is half-integer. The expressions will be used to see if any multipoles can be identified by the angular distributions.

X. INTERPRETATION

As pointed out in section VIII there is a rise in the total cross section above k = 600 Mev. If the interpretation that this is a broad peak which starts at 600 Mev. is correct, the dotted curve in figure 24 shows that its value is about 10 ^{o}/o of the value of the (3, 3) resonance peak. The peak in the I = 1/2 total pion-nucleon scattering cross section obtained by Cool, Piccioni and Clark (22) occurs at 800 Mev. pion laboratory energy and has a full width at half maximum of approximately 600 Mev. They have concluded that their data are consistent with scattering in a state of j = 5/2. The corresponding peak in photoproduction should occur at k = 950 Mev.; this is certainly consistent with the data of this experiment, and it will be interesting to investigate further the possible connection between these two phenomena.

The fact that A_3 and A_4, the angular distribution coefficients, become non-zero around 600 Mev. suggests the possibility that a higher value multipole might be associated with the rise in total cross section. A non-zero A_4 term can only occur if the meson is produced in a $j \geq 5/2$ state. By the use of equations IX 24 - 29 it is possible to obtain relations between the various coefficients A_n if only one or two multipoles are important. Judging from the behavior of the total cross section, the multipole responsible for the (3, 3) resonance, M_{1+}, is large enough above 600 Mev. that it should not be neglected. If one assumes the only other non-zero multipole is one leading to a j = 5/2 state, the only choice is E_{2+} since A_4 is positive (at least below

900 Mev.). With this choice one obtains the relations

$$A_1/A_3 = -0.6 \tag{1}$$

$$A_4 = \frac{3A_o + 5A_2}{9} \tag{2}$$

Although equation 1 is consistent with the data, equation 2 is definitely not consistent. Since A_2 tends to go further negative between 600 and 800 Mev., an examination of equation IX-27 shows that the only non-interference term besides M_{1+} which will do this is E_{2-}. If one takes M_{1+}, E_{2+} and E_{2-} as the only multipoles of any consequence, then by evaluating the contribution of the M_{1+} by means of the resonance tail contribution, the values of the other multipoles can be obtained from the value of the A_n's. Within the errors, which are large, this model gives results which are reasonable. The effects of E_{2-} are dominant below 800 Mev. and then the effects of E_{2+} become dominant. However until there is some good theoretical guide, not much significance can be attached to an interpretation of this kind. Certainly the change in the angular distribution between 785 and 940 Mev. is indicative of some effect. The only conclusion that seems reasonable is that there is no one dominant multipole responsible for the rise in the cross section. The fact that A_4 is non-zero suggests that D wave mesons in a $j = 5/2$ state are produced.

On the basis of this experiment alone, one cannot make any isotopic spin assignment. When the results of the charged photomeson production from hydrogen are available, it is possible that an isotopic

spin assignment can be made. A reference to equations IX-1 and 2 shows that the charged meson production contains a larger contribution of the I = 1/2 state than the π^o reaction. Thus it will be interesting to combine the present data with data on π^+ photoproduction to see if the rise above 600 Mev. can be attributed to the state of I = 1/2.

Since this experiment became involved with meson pair production, it is probably appropriate to list the experimental evidence obtained at this laboratory about the ratio of double to single meson production. The only experiments available are this one and that of Bloch and Sands (11) which has been discussed in connection with the pair correction. They have obtained a total cross section of $56 \pm 17 \times 10^{-30} cm^2$ which is roughly constant in the energy region between 600 and 1000 Mev. The discussion in section VII gave the evidence that the reaction

$$\gamma + P \longrightarrow \pi^o + \pi^o + P \qquad (3)$$

was much less than

$$\gamma + P \longrightarrow \pi^+ + \pi^- + P \qquad (4)$$

A reasonable number for the total cross section of the two reactions is $70 \times 10^{-30} cm^2$. If one assumes that the cross section for the reaction

$$\gamma + P \longrightarrow \pi^+ + N \qquad (5)$$

is roughly the same as the reaction studied in this experiment, then

the minimum ratio of double to single production in hydrogen is about 1 in the energy region 600 - 1000 Mev. There is no experimental evidence about the reaction

$$\gamma + P \longrightarrow \pi^{o} + \pi^{+} + N \qquad (6)$$

which might make the ratio even higher. The ratio of double to single meson production in P-P collisions at a comparable available C.M. energy is only 0.25 (45). Certainly more information is needed for the photoproduction processes before a study of multiple meson production can be made.

XI. EXPERIMENTAL SUGGESTIONS

When this experiment was first begun, it was not clear that the detection of the recoil proton alone would yield good results for the single neutral meson production because of the unknown contribution of protons from meson pair production. After considering all factors, it is concluded that the method is a good one with a high enough counting rate to measure good angular distributions in a reasonable amount of machine time. The results, with the exception of a few points, are consistent and it is believed that they represent single production. There were a number of places for improvement and a discussion of these should prove valuable for the planning of future experiments on this reaction. It would be desirable to reduce the background and the pair correction and to extend the angular range of measurements.

The pulse height analysis used in this experiment was very direct and worked exceedingly well up to a momentum of 850 Mev./c. Above this value a different method would be preferable because the background from mesons produced in the Mylar walls of the target would be eliminated. A more careful shielding of the high momentum magnet counters by the use of a lead bridge from the counter house to the magnet would prevent electrons which are scattered by the air from getting into the counters. If this had been done, the use of the 1/2 inch piece of lead between the counters would not have been necessary. A great deal of time was spent measuring all the effects of this lead. If it is possible to shield the region of the external window of the target struck by the beam from the field of view of the magnet, the runs made

forward of 30^{o} will have much less background. The slit used in this experiment did a good job backward of 30^{o}. The cosmic ray background was a factor for the high momentum runs mainly because the machine was running poorly at that time; however the use of a counter in front of the magnet for high momentum runs might be useful.

The meson pair correction is only important for angles forward of 35^{o} in the lab. Since the energy spectrum of the beam is now known to have a sharp cutoff, it is possible to make the runs with lower values of E_{o} than were used in this experiment. Although a reduction in counting rate is not desirable, a smaller momentum window would reduce the correction even further. One extreme possibility is to allow the peak of the bremsstrahlung to define the upper limit of the $\Delta P \Delta \theta$ window. In this manner the pair correction can be completely eliminated for all the points run in this experiment. Unfortunately this method reduces the signal by a factor of two in the worst case but does not reduce the background.

The background for the low momentum magnet runs could have been reduced about a factor of two by the use of a lead slit. A smaller hydrogen target with a thinner Mylar cup would have reduced the scattering correction, improved the energy resolution and allowed the detection of lower energy protons with the low momentum magnet. Thus more forward π^{o} C.M. angles could be studied. The equipment exists to measure 10 Mev. protons. The detection of the recoil proton by a magnetic spectrometer is the only means of studying the π^{o} reaction at a laboratory angle of 0^{o} ($\theta'_{\pi} = 180^{o}$). The dynamics of the

reaction are such that electrons produced by the peak energy photons have a lower momentum than recoil protons which are produced in the π^o reaction by photons whose energy is somewhat below the peak energy. This very interesting region of investigation must wait until the background can be reduced to a reasonable value by the removal of much of the air path along the beam. The limitation of forward laboratory angle investigation was due to excessive background.

XII. CONCLUSIONS

It is possible to study the photoproduction of single neutral mesons from hydrogen up to photon energies of 1 Bev. by the detection of the recoil proton. A reasonable correction for the contribution of protons arising from meson pair production at forward laboratory angles can be made. Minor improvements of this method of study will reduce this correction for meson pair production and extend the angular range of measurement.

It is necessary to use terms up to $\cos^4\theta_\pi'$ to fit the angular distributions above laboratory photon energies of 600 Mev. This indicates the production of D wave mesons in a total angular momentum 5/2 state. The rise in the total cross section above 600 Mev. can be interpreted as a small broad peak which occurs in the proper energy region to be associated with the peak detected in pion-nucleon scattering measurements. This peak can not be characterized by the dominance of any single multipole absorption as is the case for the (3, 3) resonance near 300 Mev. An isotopic spin assignment must wait for the results of other experiments.

REFERENCES

1. Steinberger, Panofsky and Steller, Phys. Rev. 78, 802 (1950).
2. Steinberger, Panofsky and Steller, Phys. Rev. 86, 180 (1952).
3. A. Silverman and M. Stearns, Phys. Rev. 88, 1225 (1952).
4. G. Cocconi and A. Silverman, Phys. Rev. 88, 1230 (1952).
5. H. A. Bethe and F. deHoffmann, Mesons and Fields Vol. II, 155 (1955), Row, Peterson and Co.
6. Walker, Oakley and Tollestrup, Phys. Rev. 97, 1279 (1955).
7. D. C. Oakley and R. L. Walker, Phys. Rev. 97, 1283 (1955).
8. McDonald, Peterson and Corson, Phys. Rev. 107, 577 (1957).
9. K. A. Brueckner and K. M. Case, Phys. Rev. 83, 1141 (1951).
10. Cool, Piccioni and Clark, Phys. Rev. 103, 1082 (1956).
11. M. Bloch and M. Sands, To be published.
12. J. Mathews, Ph.D. Thesis, California Institute of Technology, (1957).
13. J. Vette and W. Wales, Low Energy Magnet Report, (May 1957), Unpublished.
14. P. L. Donoho, "A Magnetic Spectrometer for Analysis of Particles of Momentum up to 1200 Mev./c", (Nov. 1957), Unpublished.
15. D. D. Elliott, Private communication.
16. R. L. Walker, P. L. Donoho and E. B. Emery, Private communication.
17. R. Gomez, "Preliminary Calibration of the Beam Monitor of the Caltech Synchrotron", (1957), Unpublished.

18. R. R. Wilson, Preprint.

19. B. Rossi, High Energy Particles, 63 (1952), Prentice Hall Inc.

20. B. Cork, Phys. Rev. 80, 321 (1950).

21. Kruse, Teem and Ramsey, Phys. Rev. 101, 1079 (1956).

22. M. Rich and R. Madey, UCRL 2301 (1954).

23. Journal of Research of N.B.S. 41 (1948).

24. Auerbach, Bernardini, Filosofo, Hanson, Odian and Yamagata, Cern Symposium Vol. II, 291 (1956).

25. J. Mathews, Private communication.

26. S. Berman, Private communication.

27. A. M. Mood, Introduction to the Theory of Statistics, 270 (1950), McGraw-Hill Book Company, Inc.

28. W. S. McDonald, Ph.D. Thesis, California Institute of Technology, (1957).

29. M. Gell-Mann and K. M. Watson, Ann. Rev. Nuc. Sc. 4, 219 (1954).

30. N. Kemmer, Proc. Cambridge Phil. Soc. 34, 354 (1938).

31. H. A. Bethe and F. deHoffmann, Mesons and Fields, Vol. II, 111 (1955), Row, Peterson and Co.

32. K. M. Watson, Phys. Rev. 85, 852 (1952).

33. Chew, Goldberger, Low and Nambu, Phys. Rev. 106, 1345 (1957).

34. Panofsky, Aamodt and Hadley, Phys. Rev. 81, 565 (1951).

35. Brueckner, Serber and Watson, Phys. Rev. 81, 575 (1951).

36. C. N. Yang, Phys. Rev. 77, 242 (1950).

37. B. T. Feld, Phys. Rev. 89, 330L (1953).

38. K. M. Watson, Phys. Rev. 95, 228 (1954).

39. Watson, Keck, Tollestrup and Walker, Phys. Rev. 101, 1159 (1956).

40. G. F. Chew and F. E. Low, Phys. Rev. 101, 1570 (1956).

41. G. F. Chew and F. E. Low, Phys. Rev. 101, 1579 (1956).

42. L. J. Koester, Jr. and F. E. Mills, Phys. Rev. 105, 1900 (1957).

43. Walker, Hushfar and Shepard, Phys. Rev. 104, 526 (1956).

44. M. J. Moravcsik, Phys. Rev. 104, 1451 (1956).

45. Fowler, Shutt, Thorndike and Whittemore, Phys. Rev. 103, 1479 (1956).